Decay $B_c^+ \to D_{(s)}^{(*)+}\ell^+\ell^-$ within covariant confined quark model

M. A. Ivanov,[1,*] J. N. Pandya,[2,†] P. Santorelli,[3,4,‡] and N. R. Soni[4,5,§]

[1]*Bogoliubov Laboratory of Theoretical Physics, Joint Institute for Nuclear Research, 141980 Dubna, Russia*

[2]*Department of Physics, Sardar Patel University, Vallabh Vidyanagar 388120, Gujarat, India*

[3]*Dipartimento di Fisica "E. Pancini," Università di Napoli Federico II—Complesso Universitario di Monte S. Angelo Edificio 6, via Cintia, 80126 Napoli, Italy*

[4]*INFN sezione di Napoli—Complesso Universitario di Monte S. Angelo Edificio 6, via Cintia, 80126 Napoli, Italy*

[5]*Department of Physics, Faculty of Science, The Maharaja Sayajirao University of Baroda, Vadodara 390002, Gujarat, India*

(Received 25 April 2024; accepted 3 October 2024; published 4 November 2024)

We study the rare semileptonic decays of B_c mesons within the effective field theoretical framework of covariant confined quark model. The transition form factors corresponding to $B_c^+ \to D^{(*)+}$ and $B_c^+ \to D_s^{(*)+}$ are computed in the entire q^2 range. Using form factors, we compute the branching fractions and compare them with the available theoretical results. We also compute various physical observables such as forward-backward asymmetry, longitudinal and transverse polarizations, as well as clean angular observables.

DOI: 10.1103/PhysRevD.110.096003

I. INTRODUCTION

B_c meson is an interesting meson having both heavy quarks with different flavor and the mass below $B\bar{D}$ threshold. Sometimes it is also considered to be in the heavy quarkonia sector, however unlike charmonia and bottomonia B_c meson can decay through the weak interactions only. This can also be justified by the lifetime of the B_c meson and consequently, it serves as one of the best candidate for the hunt of new physics beyond the standard model. Semileptonic decay of B meson corresponding to the transition $b \to c\ell\nu_\ell$ is explored in great depth by experimental facilities worldwide and it is observed that their results are deviating from the standard model predictions [1–7]. LHCb has also reported semileptonic decay of B_c meson and ratio of branching fractions $R(J/\psi) = \mathcal{B}(B_c \to J/\psi\tau^+\nu_\tau)/\mathcal{B}(B_c \to J/\psi\mu^+\nu_\mu) = 0.71 \pm 0.17(\text{stat}) \pm 0.18(\text{syst})$ [8]. Following this observation, HPQCD collaboration performed the computation of observables corresponding to the lepton flavor universality violation from lattice QCD and determined the ratio $R(J/\psi) = 0.2582(38)$ which is found to be smaller than LHCb measurement at 1.8σ [9].

However, rare semileptonic decays are yet to be fully explored by the experimental side. In the past, several anomalies have been reported in $B \to K^{(*)}\ell\ell$ corresponding to the $b \to s\ell\ell$ channel. Several experimental facilities worldwide including LHCb, Belle, *BABAR* have provided information regarding this channels in great detail [10–12]. Further, $B_s \to \phi\ell\ell$ has also been observed by some of these collaborations. The key observations include the ratio $R_{K^{(*)}} = \mathcal{B}(B \to K^{(*)}\mu^+\mu^-)/\mathcal{B}(B \to K^{(*)}e^+e^-)$ and some other observables viz. forward-backward asymmetry, polarization and different angular observables that are deviating by $2-3\sigma$ from the standard model predictions [13–26]. These observations essentially lead to the search for the new physics beyond standard model which are discussed in the literature using the framework of light cone sum rules [27,28], effective theories [29–35] and several other theoretical approaches. In recent experimental developments, simultaneous measurements of R_K and R_{K^*} in low and central q^2 range corresponding to $q^2 \in [0.1, 1.1]\ \text{GeV}^2/\text{c}^4$ and $q^2 \in [1.1, 6]\ \text{GeV}^2/\text{c}^4$ show very good agreement with standard model predictions at 0.2σ by LHCb collaboration [36,37].

On the same lines, $b \to d\ell\ell$ can also be a potential mode for the search of new physics. For the transition corresponding to the $b \to d$, LHCb and Belle collaborations

*Contact author: ivanovm@theor.jinr.ru
†Contact author: jnpandya-phy@spuvvn.edu
‡Contact author: pietro.santorelli@na.infn.it
§Contact author: nakulphy@gmail.com

have provided some important data for the channels $B \to (\rho, \omega, \pi, \eta)\ell^+\ell^-$ and $B_s^0 \to \bar{K}^{*0}\mu^+\mu^-$ [38–40]. Further, LHCb collaboration has also provided the relative ratios for $b \to d/b \to s$ transition in the channels $\mathcal{B}(B^+ \to \pi^+\mu^+\mu^-)/\mathcal{B}(B^+ \to K^+\mu^+\mu^-)$ and $\mathcal{B}(B_s^0 \to \bar{K}^{*0}\mu^+\mu^-)/\mathcal{B}(\bar{B}^0 \to \bar{K}^{*0}\mu^+\mu^-)$ [41,42]. Several anomalies regarding these studies are reported in the book [43] and in the review article [44] including references therein.

All these anomalies can also be tested in the rare semileptonic decay of B_c meson where the decay channels $B_c^+ \to D^{(*)+}\ell^+\ell^-$ and $B_c^+ \to D_s^{(*)+}\ell^+\ell^-$ can also prove to be promising candidates for the search toward any new physics beyond the standard model. These modes are yet to be identified precisely by the experimental facilities as well as by the lattice simulations. Less availability of data on rare semileptonic branching fractions might be due to the difficulty in probing them in presence of background data of other simultaneous prominent decays. Also, B_c mesons are produced less frequently in comparison to other bottom mesons and so the higher excited states are not very well observed yet. Very recently, LHCb collaboration has also set an upper limit for $f_c/f_u \times \mathcal{B}(B_c^+ \to D_s^+\mu^+\mu^-)$ at confidence level of 95% where f_c and f_u are fragmentation fractions of a B meson with a c and u quark respectively in proton-proton collisions [45]. Whereas on the theoretical front, semileptonic as well as rare semileptonic decays are explored using various approaches as follows. Geng *et al.*, studied rare semileptonic decays using light front quark model and constituent quark model [46]. Azizi *et al.*, also studied these channels using the three point QCD sum rules [47,48]. Faessler *et al.*, also studied the exclusive rare decays $B_c \to D^{(*)}\ell\ell$ using the relativistic quark model [49]. Choi studied the transition form factors and different physical observables using the light front quark model [50]. These rare decays are studied using the perturbative QCD approach [51] as well as using the framework of single universal extra dimension [52]. Rare semileptonic decays of B and B_c mesons are also studied using the relativistic quark model RQM [53]. The transition form factors computed in the relativistic quark model [53] are also employed for study of rare semileptonic decays with non universal Z' effect [54] as well as using two Higgs doublet model [55]. Further, these form factors are also employed for the search of new physics in terms of different observables [56–58].

In the present work, we study the rare semileptonic decays for the channels $B_c^+ \to D_{(s)}^{(*)+}\ell^+\ell^-$ for $\ell = e$, μ, τ and ν which are essentially the transitions corresponding to $b \to d(s)\ell^+\ell^-$. The necessary transition form factors are computed in the entire range of momentum transfer squared by employing the covariant confined quark model (CCQM) with built-in infrared confinement leading to computation of branching fractions. We also compute some more physical observables such as forward-backward asymmetry, longitudinal and transverse polarizations as well as different other angular observables. We also compare our findings with the available experimental data and theoretical predictions. In the past, we have successfully employed CCQM for predicting various transitions for charm as well as bottom hadrons which shows the ingenuity and reliability of the model [59–65].

This paper is organized in the following way: After the brief introduction to the subject with the recent literature reports in Sec. I, we introduce theoretical model, i.e., covariant confined quark model (CCQM) in Sec. II. In this section, we provide the Wilson coefficients and transition form factors and the relations of various observables such as branching fractions, forward-backward asymmetry, longitudinal and transverse polarizations, and angular observables. Then in Sec. IV, we list all the numerical results along with the comparison with other theoretical approaches. Finally, we summarize the present work in Sec. V.

II. THEORETICAL FRAMEWORK

Within the standard model (SM), the effective Hamiltonian for the $b \to q\ell^+\ell^-$ decay can be written in terms of the following operators [66–68]

$$\mathcal{H}_{\rm eff}^{\rm SM} = -\frac{4G_F}{\sqrt{2}} V_{tq}^* V_{tb} \left\{ \sum_{i=1}^{10} C_i(\mu)\mathcal{O}_i(\mu) + \frac{V_{ub}^* V_{uq}}{V_{tb}^* V_{tq}} \sum_{i=1}^{2} C_i(\mu)[\mathcal{O}_i(\mu) - \mathcal{O}_i^u(\mu)] \right\}, \tag{1}$$

where $q = d$ for $b \to d\ell^+\ell^-$ and $q = s$ for $b \to s\ell^+\ell^-$.

In the above equation, C_i are the Wilson coefficients and the set of local operators $\mathcal{O}_i$ obtained within the SM for $b \to s\ell^+\ell^-$ as well for $b \to d\ell^+\ell^-$ transition using a standard procedure [67,68]. These operators include current-current operators ($\mathcal{O}_{1,2}$), QCD penguin operators ($\mathcal{O}_{3-6}$), dipole operators ($\mathcal{O}_{7,8}$) and electroweak semileptonic penguin operators ($\mathcal{O}_{9,10}$). Within the SM, these operators $\mathcal{O}_i$ and $\mathcal{O}_i^u$ defined as

$$\begin{aligned}
\mathcal{O}_1^u &= (\bar{q}_{a_1}\gamma^\mu P_L u_{a_2})(\bar{u}_{a_2}\gamma_\mu P_L b_{a_1}), & \mathcal{O}_2^u &= (\bar{q}\gamma^\mu P_L u)(\bar{u}\gamma_\mu P_L b),\\
\mathcal{O}_1 &= (\bar{q}_{a_1}\gamma^\mu P_L c_{a_2})(\bar{c}_{a_2}\gamma_\mu P_L b_{a_1}), & \mathcal{O}_2 &= (\bar{q}\gamma^\mu P_L c)(\bar{c}\gamma_\mu P_L b),\\
\mathcal{O}_3 &= (\bar{q}\gamma^\mu P_L b)\sum_{q'}(\bar{q}'\gamma_\mu P_L q'), & \mathcal{O}_4 &= (\bar{q}_{a_1}\gamma^\mu P_L b_{a_2})\sum_{q'}(\bar{q}'_{a_2}\gamma_\mu P_L q'_{a_1}),
\end{aligned}$$

$$\mathcal{O}_5 = (\bar{q}\gamma^\mu P_L b)\sum_{q'}(\bar{q}'\gamma_\mu P_R q'), \qquad \mathcal{O}_6 = (\bar{q}_{a_1}\gamma^\mu P_L b_{a_2})\sum_{q'}(\bar{q}'_{a_2}\gamma_\mu P_R q'_{a_1}),$$
$$\mathcal{O}_7 = \frac{e}{16\pi^2}\bar{m}_b(\bar{q}\sigma^{\mu\nu}P_R b)F_{\mu\nu}, \qquad \mathcal{O}_8 = \frac{g}{16\pi^2}\bar{m}_b(\bar{q}_{a_1}\sigma^{\mu\nu}P_R \mathbf{T}_{a_1 a_2} b_{a_2})\mathbf{G}_{\mu\nu},$$
$$\mathcal{O}_9 = \frac{e^2}{16\pi^2}(\bar{q}\gamma^\mu P_L b)(\bar{\ell}\gamma_\mu \ell), \qquad \mathcal{O}_{10} = \frac{e^2}{16\pi^2}(\bar{q}\gamma^\mu P_L b)(\bar{\ell}\gamma_\mu\gamma_5 \ell), \tag{2}$$

Here, $G_{\mu\nu}$ is the gluon field strength, $F_{\mu\nu}$ is the photon field strength, $a_{1,2}$ denote the color indices, T_{a_1,a_2} are the SU(3) color generators, $P_{L,R}$ are the chirality projection operator and μ is the renormalization scale. Matrix element for the channels $B_c \to D_{(s)}^{(*)}\ell^+\ell^-$ can be written as [66,67]

$$\mathcal{M}(B_c \to D_{(s)}^{(*)}\ell^+\ell^-) = \frac{G_F\alpha}{\sqrt{2}\pi}V_{tq}^* V_{tb}\Big\{C_9^{\rm eff}\langle D_{(s)}^{(*)}|\bar{q}\gamma_\mu P_L b|B_c\rangle(\bar{\ell}\gamma^\mu\ell) + C_{10}\langle D_{(s)}^{(*)}|\bar{q}\gamma_\mu P_L b|B_c\rangle(\bar{\ell}\gamma^\mu\gamma_5\ell)$$
$$-\frac{2\bar{m}_b}{q^2}C_7^{\rm eff}\langle D_{(s)}^{(*)}|\bar{q}i\sigma^{\mu\nu}q_\nu P_R b|B_c\rangle(\bar{\ell}\gamma^\mu\ell)\Big\}, \tag{3}$$

Here $C_9^{\rm eff}(\mu)$ contains the corrections to the four-quark operators $\mathcal{O}_{1-6}$ and $\mathcal{O}_{1,2}^u$ in Eq. (1) in the form of [69–77]

$$C_9^{\rm eff}(\mu) = \xi_1 + \lambda_q^*\xi_2, \tag{4}$$

with

$$\xi_1 = C_9 + C_0 h^{\rm eff}(\hat{m}_c,\hat{s}) - \frac{1}{2}h(1,\hat{s})(4C_3+4C_4+3C_5+C_6) - \frac{1}{2}h(0,\hat{s})(C_3+3C_4) + \frac{2}{9}(3C_3+C_4+3C_5+C_6) \tag{5}$$

$$\xi_2 = [h^{\rm eff}(\hat{m}_c,\hat{s}) - h^{\rm eff}(\hat{m}_u,\hat{s})](3C_1+C_2) \tag{6}$$

where $C_0 \equiv 3C_1 + C_2 + 3C_3 + C_4 + 3C_5 + C_6$ and $\lambda_d = (V_{ub}^* V_{ud})/(V_{tb}^* V_{td})$ for the transition corresponding to the $b \to d\ell^+\ell^-$ and $\lambda_s = (V_{ub}^* V_{us})/(V_{tb}^* V_{ts})$ for the transition corresponding to the $b \to s\ell^+\ell^-$. Further, the quark-loop contribution is given by

$$h(\hat{m}_q,\hat{s}) = -\frac{8}{9}\ln\hat{m}_q + \frac{8}{27} + \frac{4}{9}x - \frac{2}{9}(2+x)|1-x|^{1/2}\begin{cases}(\ln\left|\frac{\sqrt{1-x}+1}{\sqrt{1-x}-1}\right| - i\pi), & \text{for } x \equiv \frac{4\hat{m}_q^2}{\hat{s}} < 1,\\ 2\arctan\frac{1}{\sqrt{x-1}}, & \text{for } x \equiv \frac{4\hat{m}_q^2}{\hat{s}} > 1,\end{cases}$$

and

$$h(0,\hat{s}) = \frac{8}{27} - \frac{4}{9}\ln\hat{s} + \frac{4}{9}i\pi,$$

and the functions,

$$h^{\rm eff}(\hat{m}_c,\hat{s}) = h(\hat{m}_c,\hat{s}) + \frac{3\pi}{\alpha^2 C_0}\sum_{V=J/\psi,\psi(2S),\ldots}\frac{m_V\mathcal{B}(V\to\ell^+\ell^-)\Gamma_V}{m_V^2 - q^2 - im_V\Gamma_V}, \tag{7}$$

$$h^{\rm eff}(\hat{m}_u,\hat{s}) = h(\hat{m}_u,\hat{s}) + \frac{3\pi}{\alpha^2 C_0}\sum_{V=\rho^0,\omega,\phi}\frac{m_V\mathcal{B}(V\to\ell^+\ell^-)\Gamma_V}{m_V^2 - q^2 - im_V\Gamma_V} \tag{8}$$

where $\hat{m}_q = \bar{m}_q/m_1$, $\hat{s} = q^2/m_1^2$ and α is the coupling constant considered at Z-boson mass. The nonresonant contribution is computed by ignoring the terms containing the vector resonances in Eqs. (7) and (8). The masses, total decay widths and dilepton branching fractions of vector mesons are taken from the PDG book [78]. For the present computations, we consider the next-to-next leading order Wilson coefficients from the Ref. [79] which are essentially evaluated at renormalization scale $\mu = 2M_W$ and they are computed by renormalization group equation to the hadronic scale $\mu_b = 4.8$ GeV. The values of input parameters and Wilson coefficients are tabulated in Table I.

TABLE I. Values of the input parameters [78] and Wilson coefficients [79].

m_W	$\sin^2\theta_W$	$\alpha(M_Z)$	$\bar{m}_c$	$\bar{m}_b$	$\bar{m}_t$
80.41 GeV	0.2313	1/128.94	1.27 GeV	4.68 GeV	173.3 GeV

C_1	C_2	C_3	C_4	C_5	C_6	C_7^{eff}	C_9	C_{10}
−0.2632	1.0111	−0.0055	−0.0806	0.0004	0.0009	−0.2923	4.0749	−4.3085

TABLE II. Quark masses, meson size parameters, and infrared cutoff parameter (all in GeV).

Λ_{B_c}	Λ_D	Λ_{D^*}	Λ_{D_s}	$\Lambda_{D_s^*}$
2.728 ± 0.001	1.600 ± 0.027	1.529 ± 0.009	1.748 ± 0.035	1.556 ± 0.014

$m_{u/d}$	m_s	m_c	m_b	λ
0.241	0.428	1.67	5.05	0.181

The transition form factors corresponding to the channels $B_c^+ \to D_{(s)}^{(*)+}\ell^+\ell^-$ are computed in the effective field theoretical framework of CCQM [63,80–85]. The effective Lagrangian for the interaction between meson and constituent quark can be written in the most common form as

$$\mathcal{L}_{\text{int}} = g_M M(x) \int dx_1 \int dx_2 F_M(x; x_1, x_2)\bar{q}_2(x_2)\Gamma_M q_1(x_1) + \text{H.c.} \tag{9}$$

Here, Γ_M is the Dirac matrix and can take the values according to the type of meson based on the spin. F_M is the vertex function which describes the effective finite size of the meson given by

$$F_M(x,x_1,x_2) = \delta(x - w_1x_1 - w_2x_2)\Phi_M((x_1 - x_2)^2). \tag{10}$$

Here, Φ_M is the correlation function for the constituents with masses $m_{q_{1,2}}$ and mass ratios $w_i = m_{q_i}/(m_{q_1} + m_{q_2})$. Next, we consider the vertex function to be of the form of simple Gaussian function with the effective finite size of the meson (Λ_M). The vertex function takes the form

$$\tilde{\Phi}_M(-k^2) = e^{k^2/\Lambda_M^2} \tag{11}$$

Here, quark masses ($m_{1,2}$) and size parameters (Λ_M) are the model parameters and are listed in Table II. A key feature of choosing the vertex function to have the Gaussian form is that it will make the analytical computation easier. g_M in Eq. (9) is the coupling constant which characterizes the interaction strength between quarks and the meson. In order to justify the fact that quarks are confined within the hadrons, we use compositeness condition [86,87] for determination of coupling constants. It is given by setting the renormalization constant (Z_M) to be equal to zero as,

$$Z_M = 1 - \frac{3g_M^2}{4\pi^2}\tilde{\Pi}'_M(m_M^2) = 0. \tag{12}$$

Here, $\tilde{\Pi}_M$ is the meson mass operator given in Fig. 1 defined as

$$\tilde{\Pi}_M(p^2) = N_c g_M^2 \int \frac{d^4k}{(2\pi)^4 i}\tilde{\Phi}_M^2(-k^2)\text{tr}[\Gamma_M S_1(k + w_1 p) \times \Gamma_M S_2(k - w_2 p)]. \tag{13}$$

Here, $N_c = 3$ is the number of colors and $S_{1,2}$ are the free quark propagators that can be written in the form of Fock-Schwinger representation as it provides the additional advantages for the computation of loop integration. All the necessary analytical computation including trace evaluation, loop integration were performed using the FORM

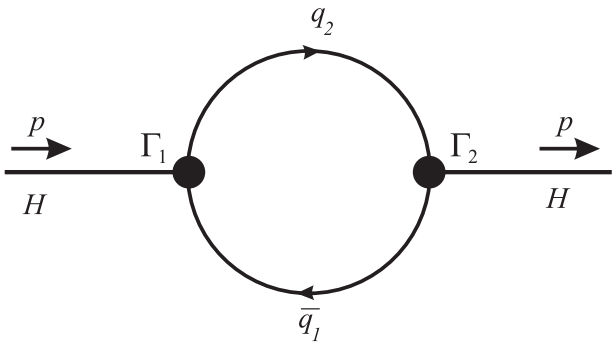

FIG. 1. Feynman diagram for meson mass operator.

language. At the end, a universal infrared confinement parameter $\lambda = 0.181$ GeV is introduced in order to avoid inclusion of divergences in the quark loop diagrams. Next, we define the CCQM model parameters such as quark masses (m_q) and size parameters Λ_M. In present work, we have utilized the updated least square fit method reported in the past CCQM Refs. [63,88–90]. In these references, the model parameters are determined by fitting the computed observables such as leptonic decay widths, electromagnetic transition widths and meson masses with the experimental data or lattice simulations and the differences are considered as the absolute uncertainty in the respective size parameters. It is important to note here that the maximum uncertainty is found to be less than 10% for the computed form factors at the maximum q^2 range. Further, these uncertainties in the form factors are then transported for the branching fraction computations and other physical observables.

With the optimized model parameters and coupling constants, we compute the transition form factors in the whole q^2 range. The transition form factors for the channels $B_c^+ \to D_{(s)}^{(*)+}$ can be written as

$$\begin{aligned}
\langle D_{(s)}(p_2)|\bar{q}O^\mu b|B_c(p_1)\rangle &= N_c g_{B_c} g_{D_{(s)}} \int \frac{d^4k}{(2\pi)^4 i} \tilde{\phi}_{B_c}(-(k+w_{13}p_1)^2)\tilde{\phi}_{D_{(s)}}(-(k+w_{23}p_2)^2) \\
&\quad \times \mathrm{tr}[O^\mu S_1(k+p_1)\gamma^5 S_3(k)\gamma^5 S_2(k+p_2)] \\
&= F_+(q^2)P^\mu + F_-(q^2)q^\mu, \\
\langle D_{(s)}(p_2)|\bar{q}\sigma^{\mu\nu}(1-\gamma^5)b|B_c(p_1)\rangle &= N_c g_{B_c} g_{D_{(s)}} \int \frac{d^4k}{(2\pi)^4 i} \tilde{\phi}_{B_c}(-(k+w_{13}p_1)^2)\tilde{\phi}_{D_{(s)}}(-(k+w_{23}p_2)^2) \\
&\quad \times \mathrm{tr}[\sigma^{\mu\nu}(1-\gamma^5)S_1(k+p_1)\gamma^5 S_3(k)\gamma^5 S_2(k+p_2)] \\
&= \frac{iF_T(q^2)}{m_1+m_2}(P^\mu q^\nu - P^\nu q^\mu + i\varepsilon^{\mu\nu Pq}).
\end{aligned} \tag{14}$$

$$\begin{aligned}
\langle D^*_{(s)}(p_2,\epsilon)|\bar{q}O^\mu b|B_c(p_1)\rangle &= N_c g_{B_c} g_{D^*_{(s)}} \int \frac{d^4k}{(2\pi)^4 i} \tilde{\phi}_{B_c}(-(k+w_{13}p_1)^2)\tilde{\phi}_{D^*_{(s)}}(-(k+w_{23}p_2)^2) \\
&\quad \times \mathrm{tr}[O^\mu S_1(k+p_1)\gamma^5 S_3(k)\not{\epsilon}^\dagger_\nu S_2(k+p_2)] \\
&= \frac{\epsilon^\dagger_\nu}{m_1+m_2}[-g^{\mu\nu}P\cdot qA_0(q^2) + P^\mu P^\nu A_+(q^2) + q^\mu P^\nu A_-(q^2) + i\varepsilon^{\mu\nu\alpha\beta}P_\alpha q_\beta V(q^2)], \\
\langle D^*_{(s)}(p_2,\epsilon)|\bar{q}\sigma^{\mu\nu}q_\nu(1+\gamma^5)b|B_c(p_1)\rangle &= N_c g_{B_c} g_{D^*_{(s)}} \int \frac{d^4k}{(2\pi)^4 i} \tilde{\phi}_{B_c}(-(k+w_{13}p_1)^2)\tilde{\phi}_{D^*_{(s)}}(-(k+w_{23}p_2)^2) \\
&\quad \times \mathrm{tr}[\sigma^{\mu\nu}q_\nu(1+\gamma^5)S_1(k+p_1)\gamma^5 S_3(k)\not{\epsilon}^\dagger_\nu S_2(k+p_2)] \\
&= \epsilon^\dagger_\nu[-(g^{\mu\nu} - q^\mu q^\nu/q^2)P\cdot q a_0(q^2) + i\varepsilon^{\mu\nu\alpha\beta}P_\alpha q_\beta g(q^2) \\
&\quad + (P^\mu P^\nu - q^\mu P^\nu P\cdot q/q^2)a_+(q^2)].
\end{aligned} \tag{15}$$

Here, P is the total momentum of the parent and daughter mesons and q is the momentum transfer between them. Polarization vector of the daughter meson is defined in such a way that $\epsilon^\dagger_\nu \cdot p_2 = 0$. $p_1^2 = m_{B_c}^2$, $p_2^2 = m^2_{D^{(*)}_{(s)}}$. With all the necessary inputs, the form factors are computed by solving the multidimensional integral using *Mathematica* in the entire range of momentum transfer squared. We plot the form factors in Eqs. (14) and (15) in Fig. 2 and also represent them in the double pole approximation as

$$F(q^2) = \frac{F(0)}{1 - a\left(\frac{q^2}{m_1^2}\right) + b\left(\frac{q^2}{m_1^2}\right)^2} \tag{16}$$

The form factors at the maximum recoil $F(0)$ and double pole parameters a and b are listed in Table III. It is important to note here that the uncertainty in the form factors for $q^2 = 0$ to $q^2 = q^2_{\max}$ are computed employing the model parameters. Further, uncertainty in the double pole parameters are extracted by performing least

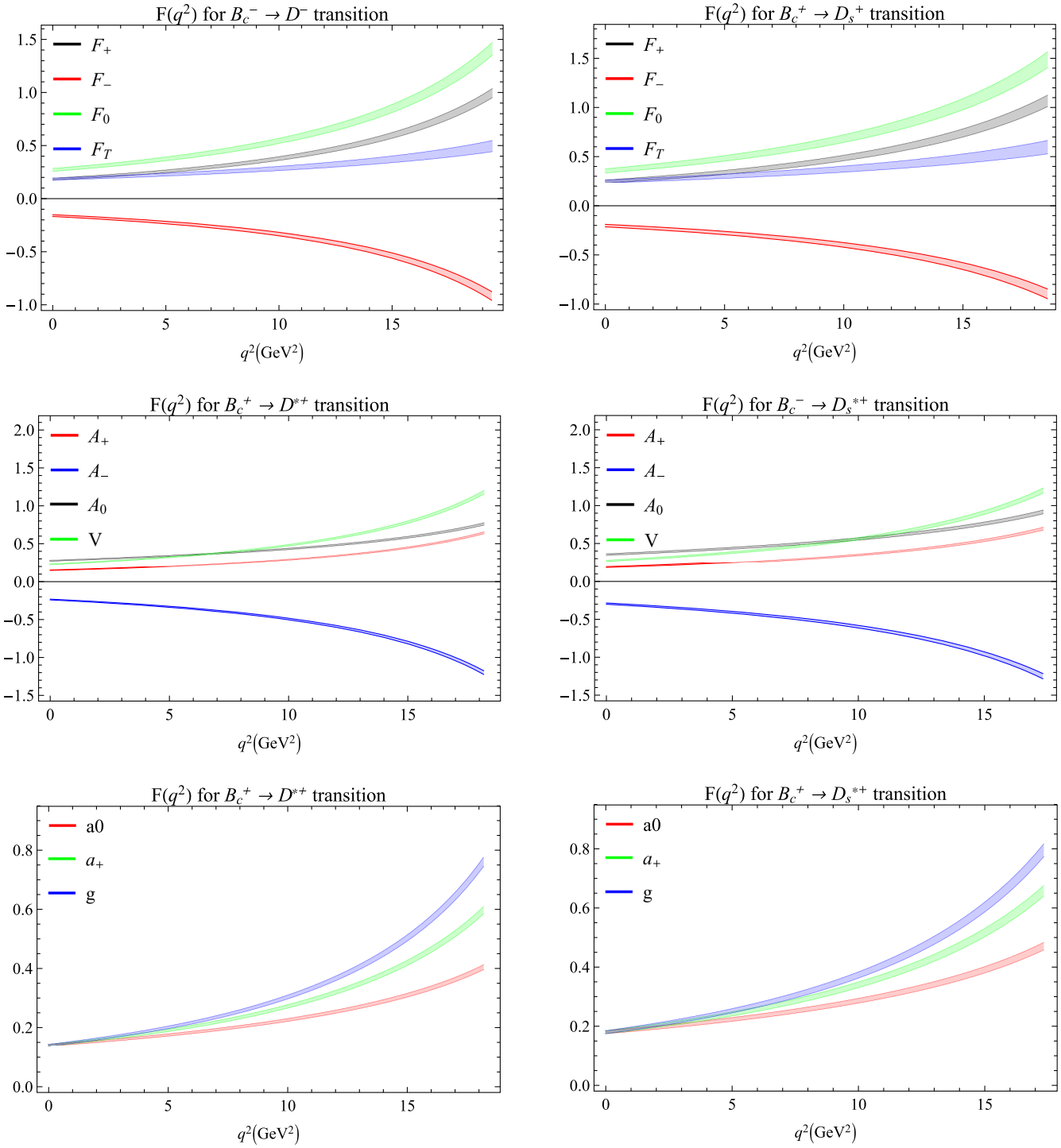

FIG. 2. Form factors.

TABLE III. Form factors and double pole parameters appeared in Eq. (16).

F	$F(0)$	a	b	F	$F(0)$	a	b
$F_+^{B_c\to D}$	0.188 ± 0.003	2.344 ± 0.012	1.422 ± 0.027	$F_-^{B_c\to D}$	$-(0.161 \pm 0.002)$	2.417 ± 0.011	1.512 ± 0.026
$F_T^{B_c\to D}$	0.274 ± 0.004	2.282 ± 0.012	1.319 ± 0.028	$F_0^{B_c\to D}$	0.187 ± 0.004	1.487 ± 0.045	0.458 ± 0.112
$A_0^{B_c\to D^*}$	0.278 ± 0.002	1.447 ± 0.010	0.171 ± 0.026	$A_+^{B_c\to D^*}$	0.152 ± 0.001	2.155 ± 0.007	1.089 ± 0.017
$A_-^{B_c\to D^*}$	$-(0.237 \pm 0.002)$	2.409 ± 0.006	1.459 ± 0.015	$V^{B_c\to D^*}$	0.232 ± 0.002	2.392 ± 0.006	1.421 ± 0.015
$a_0^{B_c\to D^*}$	0.143 ± 0.001	1.532 ± 0.010	0.294 ± 0.025	$a_+^{B_c\to D^*}$	0.143 ± 0.009	2.147 ± 0.007	1.090 ± 0.018
$g^{B_c\to D^*}$	0.144 ± 0.001	2.472 ± 0.006	1.554 ± 0.014				
$F_+^{B_c\to D_s}$	0.256 ± 0.004	2.204 ± 0.019	1.253 ± 0.046	$F_-^{B_c\to D_s}$	$-(0.203 \pm 0.004)$	2.265 ± 0.019	1.325 ± 0.045
$F_T^{B_c\to D_s}$	0.363 ± 0.006	2.152 ± 0.019	1.167 ± 0.047	$F_0^{B_c\to D_s}$	0.255 ± 0.006	1.376 ± 0.057	0.333 ± 0.149
$A_0^{B_c\to D_s^*}$	0.367 ± 0.003	1.444 ± 0.016	0.179 ± 0.041	$A_+^{B_c\to D_s^*}$	0.191 ± 0.002	2.116 ± 0.011	1.049 ± 0.029
$A_-^{B_c\to D_s^*}$	$-(0.294 \pm 0.003)$	2.347 ± 0.010	1.388 ± 0.026	$V^{B_c\to D_s^*}$	0.284 ± 0.002	2.327 ± 0.010	1.347 ± 0.026
$a_0^{B_c\to D_s^*}$	0.181 ± 0.002	1.527 ± 0.015	0.295 ± 0.039	$a_+^{B_c\to D_s^*}$	0.181 ± 0.002	2.111 ± 0.011	1.057 ± 0.029
$g^{B_c\to D_s^*}$	0.181 ± 0.002	2.397 ± 0.010	1.464 ± 0.025				

square fit with χ^2 to be minimum by employing Minuit algorithm [91]. We also provide the covariance matrix for the coefficients $F(0)$, a and b in Tables X–XIII in the Appendix for all the transitions considered here.

III. BRANCHING FRACTIONS AND OTHER PHYSICAL OBSERVABLES

Having determined form factors and Wilson coefficients, we compute the differential decay rates for rare semileptonic decays using the relation [49]

$$\frac{d\Gamma(B_c \to D_{(s)}^{(*)}\ell^+\ell^-)}{dq^2} = \frac{G_F^2}{(2\pi)^3}\left(\frac{\alpha V_{tb}^* V_{tq}}{2\pi}\right)^2 \frac{|\mathbf{p_2}| q^2 \beta_\ell}{12 m_1^2}\mathcal{H}_{\rm tot}. \tag{17}$$

Here, $\beta_\ell = \sqrt{1-4m_\ell^2/q^2}$ and $|\mathbf{p_2}| = \lambda^{1/2}(m_1^2, m_2^2, q^2)/(2m_1)$ is the momentum of the daughter meson in the rest frame of B_c meson with $\lambda(x,y,z)$ to be the Källen function. Further $m_1 = m_{B_c}$ and $m_2 = m_{D_{(s)}^*}$. $\mathcal{H}_{\rm tot}$ is the amplitude given here in terms of the helicity amplitudes

$$\mathcal{H}_{\rm tot} = \frac{1}{2}(\mathcal{H}_U^{11} + \mathcal{H}_U^{22} + \mathcal{H}_L^{11} + \mathcal{H}_L^{22}) + \left(\frac{2m_\ell^2}{q^2}\right)\left(\frac{1}{2}\mathcal{H}_U^{11} - \mathcal{H}_U^{22} + \frac{1}{2}\mathcal{H}_L^{11} - \mathcal{H}_L^{22} + \frac{3}{2}\mathcal{H}_S^{22}\right). \tag{18}$$

The helicity amplitudes here are presented in terms of helicity form factors via the relations for the channels $B_c \to D_{(s)}$ as [49,61]

$$\mathcal{H}_U^{ii} = 0, \qquad \mathcal{H}_L^{ii} = |H_0^i|^2, \qquad \mathcal{H}_S^{ii} = |H_{t0}^i|^2. \tag{19}$$

with $i = 1, 2$ and these helicity form factors are related to the invariant form factors via

$$H_0^i = \frac{2m_1|\mathbf{p_2}|}{\sqrt{q^2}}\mathcal{F}_+^i,$$
$$H_{t0}^i = \frac{1}{\sqrt{q^2}}((m_1^2 - m_2^2)\mathcal{F}_+^i + q^2\mathcal{F}_-^i). \tag{20}$$

The invariant form factors $\mathcal{F}_{+-}^i$ for $i = 1, 2$ are related to the form factors in Eq. (14) as

$$\mathcal{F}_+^1 = C_9^{\rm eff}F_+ + C_7^{\rm eff}F_T\frac{2\bar{m}_b}{m_1+m_2},$$
$$\mathcal{F}_-^1 = C_9^{\rm eff}F_- - C_7^{\rm eff}F_T\frac{2\bar{m}_b}{m_1+m_2}\frac{m_1^2-m_2^2}{q^2},$$
$$\mathcal{F}_+^2 = C_{10}F_+, \qquad \mathcal{F}_-^2 = C_{10}F_-. \tag{21}$$

Similarly, helicity amplitudes are presented in terms of helicity form factors via relations for the channels $B_c \to D_{(s)}^*$ as [49,61]

$$\mathcal{H}_U^{ii} = |H_{+1+1}^i|^2 + |H_{-1-1}^i|^2,$$
$$\mathcal{H}_L^{ii} = |H_{00}^i|^2, \qquad \mathcal{H}_S^{ii} = |H_{t0}^i|^2, \tag{22}$$

and these helicity form factors are related to the invariant form factors via

$$H^i_{t0} = \frac{1}{m_1+m_2}\frac{m_1|\mathbf{p_2}|}{m_2\sqrt{q^2}}(Pq(-A^i_0+A^i_+)+q^2A^i_-),$$
$$H^i_{\pm1\pm1} = \frac{1}{m_1+m_2}(-PqA^i_0 \pm 2m_1|\mathbf{p_2}|V^i),$$
$$H^i_{00} = \frac{1}{m_1+m_2}\frac{1}{2m_2\sqrt{q^2}} \times (-Pq(m_1^2-m_2^2-q^2)A^i_0+4m_1^2|\mathbf{p_2}|^2A^i_+). \quad (23)$$

The invariant form factors A^i and V^i $(i=1,2)$ are related to the form factors in Eq. (15) as

$$V^{(1)} = C_9^{\rm eff}V + C_7^{\rm eff}g\frac{2\bar{m}_b(m_1+m_2)}{q^2},$$
$$A_0^{(1)} = C_9^{\rm eff}A_0 + C_7^{\rm eff}a_0\frac{2\bar{m}_b(m_1+m_2)}{q^2},$$
$$A_+^{(1)} = C_9^{\rm eff}A_+ + C_7^{\rm eff}a_+\frac{2\bar{m}_b(m_1+m_2)}{q^2},$$
$$A_-^{(1)} = C_9^{\rm eff}A_- + C_7^{\rm eff}(a_0-a_+)\frac{2\bar{m}_b(m_1+m_2)}{q^2}\frac{Pq}{q^2},$$
$$V^{(2)} = C_{10}V, \quad A_0^{(2)} = C_{10}A_0, \quad A_\pm^{(2)} = C_{10}A_\pm. \quad (24)$$

Using above relations, we plot differential branching fractions Eq. (17) in Fig. 6 while computed branching fractions are listed in Table IV. We have computed branching fractions corresponding to the dimuon channels also and compared our findings with the results of other reported theoretical results.

The differential decay width for the transition $B_c \to D^{(*)}_{(s)}\nu\bar{\nu}$ can be written as [49,61]

$$\frac{d\Gamma(B_c^+ \to D^{(*)+}_{(s)}\nu\bar{\nu})}{dq^2} = \frac{G_F^2}{(2\pi)^3}\left(\frac{\alpha V^*_{tb}V_{tq}}{2\pi}\right)^2\left[\frac{D_\nu(x_t)}{\sin^2\theta_W}\right]^2 \times \frac{|\mathbf{p_2}|q^2}{4m_1^2}(H_U+H_L), \quad (25)$$

where $x_t = m_t^2/m_W^2$ and the function $D_\nu(x_t)$ can be written up to NLO correction as [92–95]

$$D_\nu(x) = D_0(x) + \frac{\alpha_s}{4\pi}D_1(x) \quad (26)$$

with

$$D_0(x) = \frac{x}{8}\left(\frac{2+x}{x-1} + \frac{3x-6}{(x-1)^2}\ln x\right) \quad (27)$$

TABLE IV. Branching fractions of $B_c^+ \to D^{(*)+}_{(s)}\ell^+\ell^-$ for $\ell = e$, μ, and τ.

Channel	Without resonances	With resonances	LFQM [46]	CQM [46]	pQCD [51]	RQM [53]
$10^9\mathcal{B}(B_c^+ \to D^+e^+e^-)$	3.457 ± 0.125	2.665 ± 0.065	4.100	4.000	⋯	⋯
$10^9\mathcal{B}(B_c^+ \to D^+\mu^+\mu^-)$	3.449 ± 0.125	2.659 ± 0.065	4.100	4.000	3.790	3.700
$10^9\mathcal{B}(B_c^+ \to D^+\tau^+\tau^-)$	0.730 ± 0.070	0.503 ± 0.056	1.300	1.200	1.030	1.500
$10^8\mathcal{B}(B_c^+ \to D^+\nu^+\nu^-)$	1.386 ± 0.048	⋯	2.770	2.740	3.130	2.160
$10^9\mathcal{B}(B_c^+ \to D^{*+}e^+e^-)$	7.031 ± 0.215	4.983 ± 0.095	10.100	7.900	⋯	⋯
$10^9\mathcal{B}(B_c^+ \to D^{*+}\mu^+\mu^-)$	5.934 ± 0.161	3.894 ± 0.070	10.100	7.900	12.100	8.100
$10^9\mathcal{B}(B_c^+ \to D^{*+}\tau^+\tau^-)$	0.718 ± 0.025	0.518 ± 0.019	1.800	1.400	1.600	1.900
$10^8\mathcal{B}(B_c^+ \to D^{*+}\nu^+\nu^-)$	2.572 ± 0.089	⋯	7.640	5.990	11.000	5.120
$10^7\mathcal{B}(B_c^+ \to D^{*+}\gamma)$	1.235 ± 0.017	⋯	⋯	⋯	⋯	⋯
$10^7\mathcal{B}(B_c^+ \to D_s^+e^+e^-)$	1.243 ± 0.055	0.797 ± 0.024	1.360	1.330	⋯	⋯
$10^7\mathcal{B}(B_c^+ \to D_s^+\mu^+\mu^-)$	1.239 ± 0.055	0.793 ± 0.024	1.360	1.330	1.560	1.160
$10^7\mathcal{B}(B_c^+ \to D_s^+\tau^+\tau^-)$	0.207 ± 0.024	0.136 ± 0.018	0.340	0.370	0.380	0.330
$10^7\mathcal{B}(B_c^+ \to D_s^+\nu^+\nu^-)$	4.979 ± 0.210	⋯	9.200	9.200	0.129	6.500
$10^7\mathcal{B}(B_c^+ \to D_s^{*+}e^+e^-)$	2.311 ± 0.104	1.558 ± 0.055	4.090	2.810	⋯	⋯
$10^7\mathcal{B}(B_c^+ \to D_s^{*+}\mu^+\mu^-)$	1.913 ± 0.070	1.162 ± 0.028	4.090	2.810	4.400	2.120
$10^7\mathcal{B}(B_c^+ \to D_s^{*+}\tau^+\tau^-)$	0.173 ± 0.008	0.144 ± 0.007	0.510	0.410	0.520	0.350
$10^7\mathcal{B}(B_c^+ \to D_s^{*+}\nu^+\nu^-)$	8.340 ± 0.393	⋯	31.200	21.200	40.400	13.500
$10^6\mathcal{B}(B_c^+ \to D_s^{*+}\gamma)$	4.454 ± 0.098	⋯	⋯	⋯	⋯	⋯

$$D_1(x) = -\frac{29x - x^2 - 4x^3}{3(1-x)^2} - \frac{x + 9x^2 - x^3 - x^4}{(1-x)^3}\ln x + \frac{8x + 4x^2 + x^3 - x^4}{2(1-x)^3}\ln^2 x - \frac{4x - x^3}{(1-x)^2}\int_1^x dt\frac{\ln t}{1-t} + 8x\frac{\partial D_0(x)}{\partial x}\ln\left(\frac{\mu_b^2}{m_W^2}\right). \quad (28)$$

As in the previous case, the helicity amplitudes are related to helicity form factors for the channels $B_c^+ \to D_{(s)}^+\nu\bar{\nu}$ as [49,61]

$$\mathcal{H}_L = |H_0|^2, \qquad \mathcal{H}_U = 0 \quad (29)$$

with

$$H_0 = \frac{2m_1|\mathbf{p}_2|}{\sqrt{q^2}}F_+. \quad (30)$$

instead for the channels $B_c^+ \to D_{(s)}^{*+}\nu\bar{\nu}$ as [49,61]

$$\mathcal{H}_U = |H_{+1+1}|^2 + |H_{-1-1}|^2, \qquad \mathcal{H}_L = |H_{00}|^2, \quad (31)$$

with

$$H_{\pm1\pm1} = \frac{1}{m_1+m_2}(-Pq A_0 \pm 2m_1|\mathbf{p_2}|V),$$
$$H_{00} = \frac{1}{m_1+m_2}\frac{1}{2m_2\sqrt{q^2}}(-Pq(m_1^2 - m_2^2 - q^2)A_0 + 4m_1^2|\mathbf{p_2}|^2 A_+). \quad (32)$$

The numerical results on the branching fractions are listed in Table IV in comparison with the results of other theoretical approaches.

We further compute other physical observables such as forward-backward asymmetry, longitudinal and transverse polarizations and other clean observables. These lepton flavor dependent angular observables are related with the helicity amplitudes as well as corresponding form factors. Experimental measurements of these observables have played critical role in search for new physics beyond the SM for the transition $b \to s\ell\ell$ corresponding to the channel $B \to K^*\ell\ell$ by LHCb [19,96] and Belle collaborations [97]. Angular analysis are also observed for the channel $B_s \to \phi\mu^+\mu^-$ and $\Lambda_b^0 \to \Lambda\mu^+\mu^-$ by LHCb collaboration [98,99]. However, in other channels, these observables are yet to be identified. Many of these experimental measurements seem to deviate from the SM predictions and explained using new physics scenario [100–106]. Similar behavior is expected in case of $b \to d\ell\ell$ transitions. These observables could be helpful in studying the effects of CP violation. Very recently in Ref. [107], these angular observables are computed using the covariant light front quark model where transition form factors are obtained using modified Godfrey-Isgur model for the channel $B_c \to D_s^*\ell\ell$. The same observables are also studied for the channels $\bar{B}_s \to K^*\ell\ell$ and $\bar{B} \to \rho\ell\ell$ using light cone sum rule approach [108]. Recently, some of us have studied these observables in the $b \to d\ell^+\ell^-$ [61] transition. They are described in terms of four-fold angular distribution and expressed explicitly in terms of helicity form factors. The detailed description and computation techniques of these observables can be found in the Refs. [109,110]. Relation for these observables reads as

(1) Forward-backward asymmetry

$$A_{\rm FB} = \frac{1}{d\Gamma/dq^2}\left[\int_0^1 - \int_{-1}^0\right]d\cos\theta\frac{d^2\Gamma}{dq^2 d\cos\theta} = -\frac{3}{4}\beta_\ell\frac{\mathcal{H}_P^{12}}{\mathcal{H}_{\rm tot}}. \quad (33)$$

(2) Longitudinal and transverse polarization fractions

$$F_L = \frac{1}{2}\beta_\ell^2\frac{\mathcal{H}_L^{11} + \mathcal{H}_L^{22}}{\mathcal{H}_{\rm tot}}, \quad F_T = \frac{1}{2}\beta_\ell^2\frac{\mathcal{H}_U^{11} + \mathcal{H}_U^{22}}{\mathcal{H}_{\rm tot}}. \quad (34)$$

(3) Clean observables

$$\langle P_1\rangle_{\rm bin} = -2\frac{\int_{\rm bin} dq^2\beta_\ell^2[\mathcal{H}_T^{11} + \mathcal{H}_T^{22}]}{\int_{\rm bin} dq^2\beta_\ell^2[\mathcal{H}_U^{11} + \mathcal{H}_U^{22}]},$$
$$\langle P_2\rangle_{\rm bin} = -\frac{\int_{\rm bin} dq^2\beta_\ell\mathcal{H}_P^{12}}{\int_{\rm bin} dq^2\beta_\ell^2[\mathcal{H}_U^{11} + \mathcal{H}_U^{22}]},$$
$$\langle P_3\rangle_{\rm bin} = -\frac{\int_{\rm bin} dq^2\beta_\ell^2[\mathcal{H}_{IT}^{11} + \mathcal{H}_{IT}^{22}]}{\int_{\rm bin} dq^2\beta_\ell^2[\mathcal{H}_U^{11} + \mathcal{H}_U^{22}]},$$
$$\langle P_4'\rangle_{\rm bin} = 2\frac{\int_{\rm bin} dq^2\beta_\ell^2[\mathcal{H}_I^{11} + \mathcal{H}_I^{22}]}{N_{\rm bin}},$$
$$\langle P_5'\rangle_{\rm bin} = -2\frac{\int_{\rm bin} dq^2\beta_\ell[\mathcal{H}_A^{12} + \mathcal{H}_A^{21}]}{N_{\rm bin}},$$
$$\langle P_6'\rangle_{\rm bin} = -2\frac{\int_{\rm bin} dq^2\beta_\ell[\mathcal{H}_{II}^{12} + \mathcal{H}_{II}^{21}]}{N_{\rm bin}},$$
$$\langle P_8'\rangle_{\rm bin} = 2\frac{\int_{\rm bin} dq^2\beta_\ell^2[\mathcal{H}_{IA}^{11} + \mathcal{H}_{IA}^{22}]}{N_{\rm bin}}. \quad (35)$$

with the normalization factor $N_{\rm bin}$ defined as

$$\mathcal{N}_{\rm bin} = \sqrt{\int_{\rm bin} dq^2\beta_\ell^2[\mathcal{H}_U^{11} + \mathcal{H}_U^{22}]\cdot\int_{\rm bin} dq^2\beta_\ell^2[\mathcal{H}_L^{11} + \mathcal{H}_L^{22}]}. \quad (36)$$

For computation of expectation value of these observables over bins, we need to multiply them by the phase space factor $|\mathbf{p_2}|q^2\beta_\ell$ in corresponding numerator and denominator separately. The angle appearing in the relation of

forward-backward asymmetry is the polar angle between the momentum of parent meson and the momentum transfer. Further, bins are corresponding to the momentum transfer squared ranges [1.1, 6.0], [6.0, 8.0], [11.0, 12.5], and [15.0, 17.0] GeV^2.

IV. RESULTS AND DISCUSSION

Using covariant confined quark model, we compute the transition form factors using the model parameters in Table II and we plot them in terms of q^2 in Fig. 2. We also compare our form factors with the results of various other theoretical prediction such as relativistic constituent quark model (RQM) [49], constituent quark model (CQM) [46], QCD sum rules (QCDSR) [48], light front quark model (LFQM) [50], relativistic quark model (RQM) [53], perturbative QCD (pQCD) [51]. However, in order to have the comparison, we need to transform our form factors Eqs. (14) and (15) with those using BSW form factors [111]. The transformed form factors are denoted using primed symbols.

$$F_0' = F_+ + \frac{q^2}{m_1^2 - m_2^2} F_-, \tag{37}$$

$$A_0 = \frac{m_1 + m_2}{m_1 - m_2} A_1', \qquad A_+ = A_2',$$
$$A_- = \frac{2m_2(m_1 + m_2)}{q^2}(A_3' - A_0'), \qquad V = V',$$
$$a_0 = T_2', g = T_1', \qquad a_+ = T_2' + \frac{q^2}{m_1^2 - m_2^2} T_3'. \tag{38}$$

These form factors also satisfy the constraints

$$A_0'(0) = A_3'(0)$$
$$2m_2 A_3'(q^2) = (m_1 + m_2)A_1'(q^2) - (m_1 - m_2)A_2'(q^2). \tag{39}$$

For the subsequent section, we remove the prime from the form factors in order to avoid confusion. The graphical comparison between the results can be found in Figs. 3–5. It is observed that our results of the form factors for the

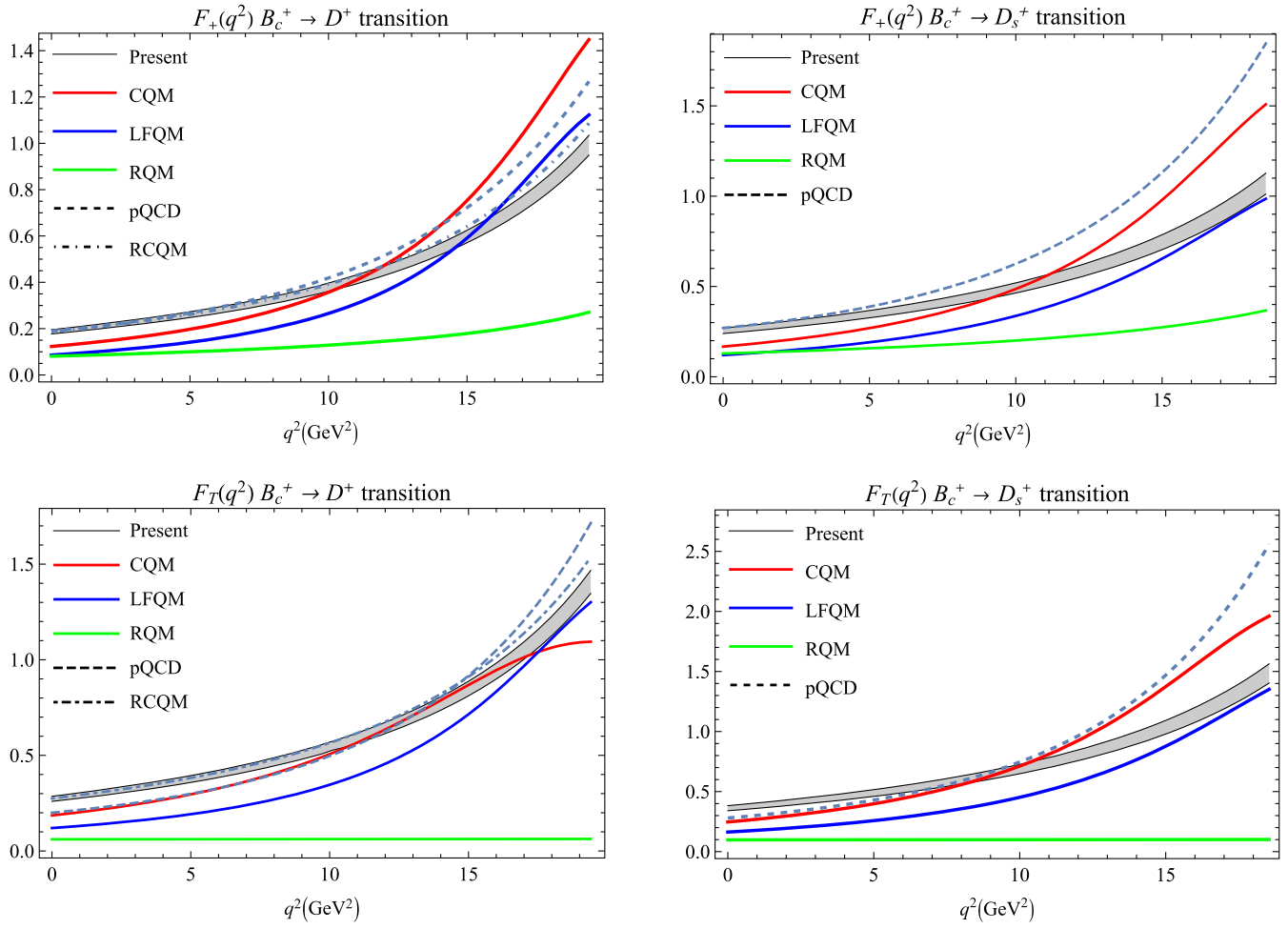

FIG. 3. Form factor comparison for $B_c \to D$ (left) and $B_c \to D_s$ (right) in comparison with relativistic constituent quark model [49], constituent quark model [46], light front quark model [50], relativistic quark model [53] and perturbative QCD [51].

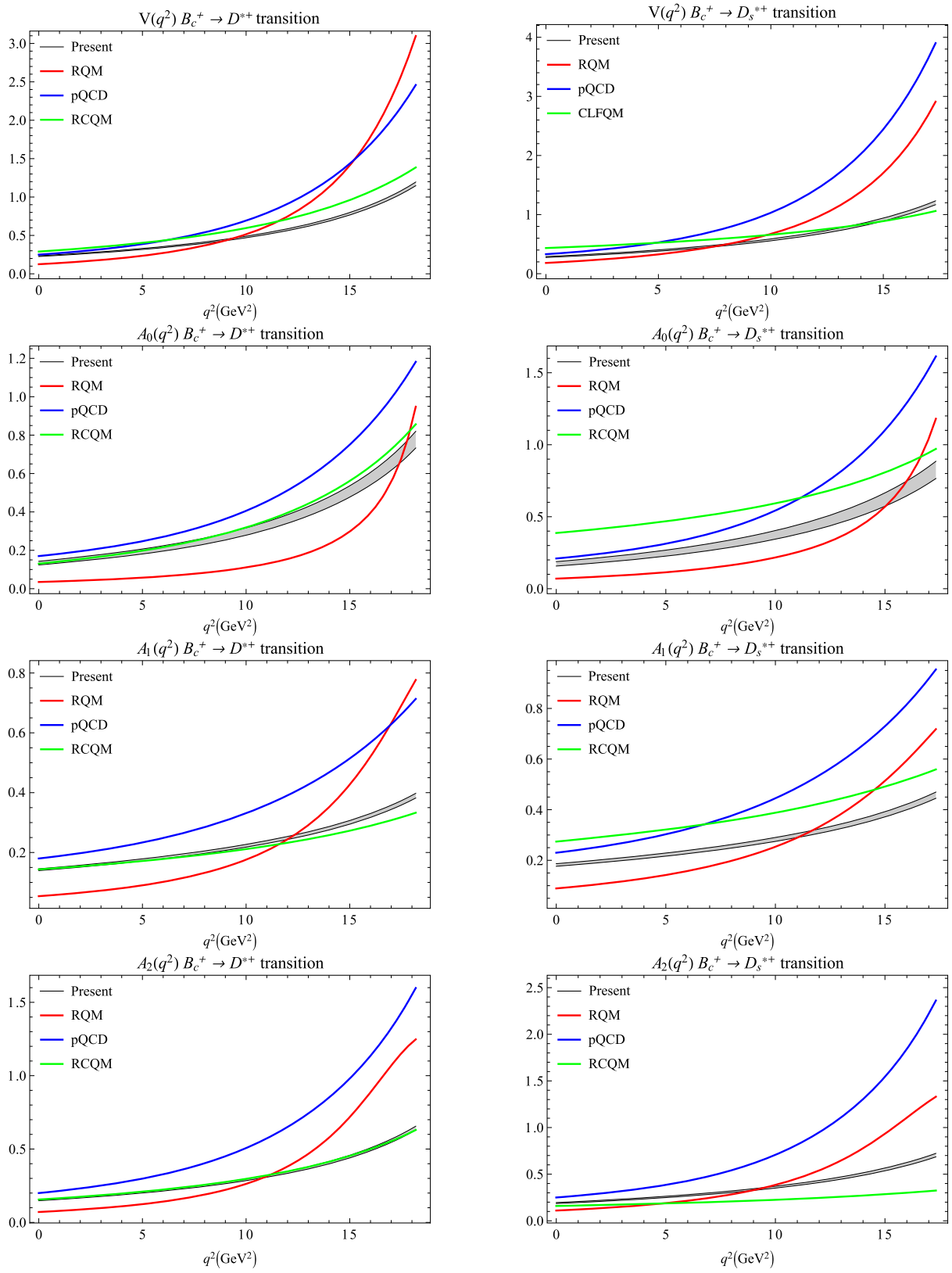

FIG. 4. Form factor comparison for $B_c \to D^*$ (left) and $B_c \to D_s^*$ (right) in comparison with relativistic constituent quark model [49], relativistic quark model [53], perturbative QCD [51], and covariant light front quark model [107].

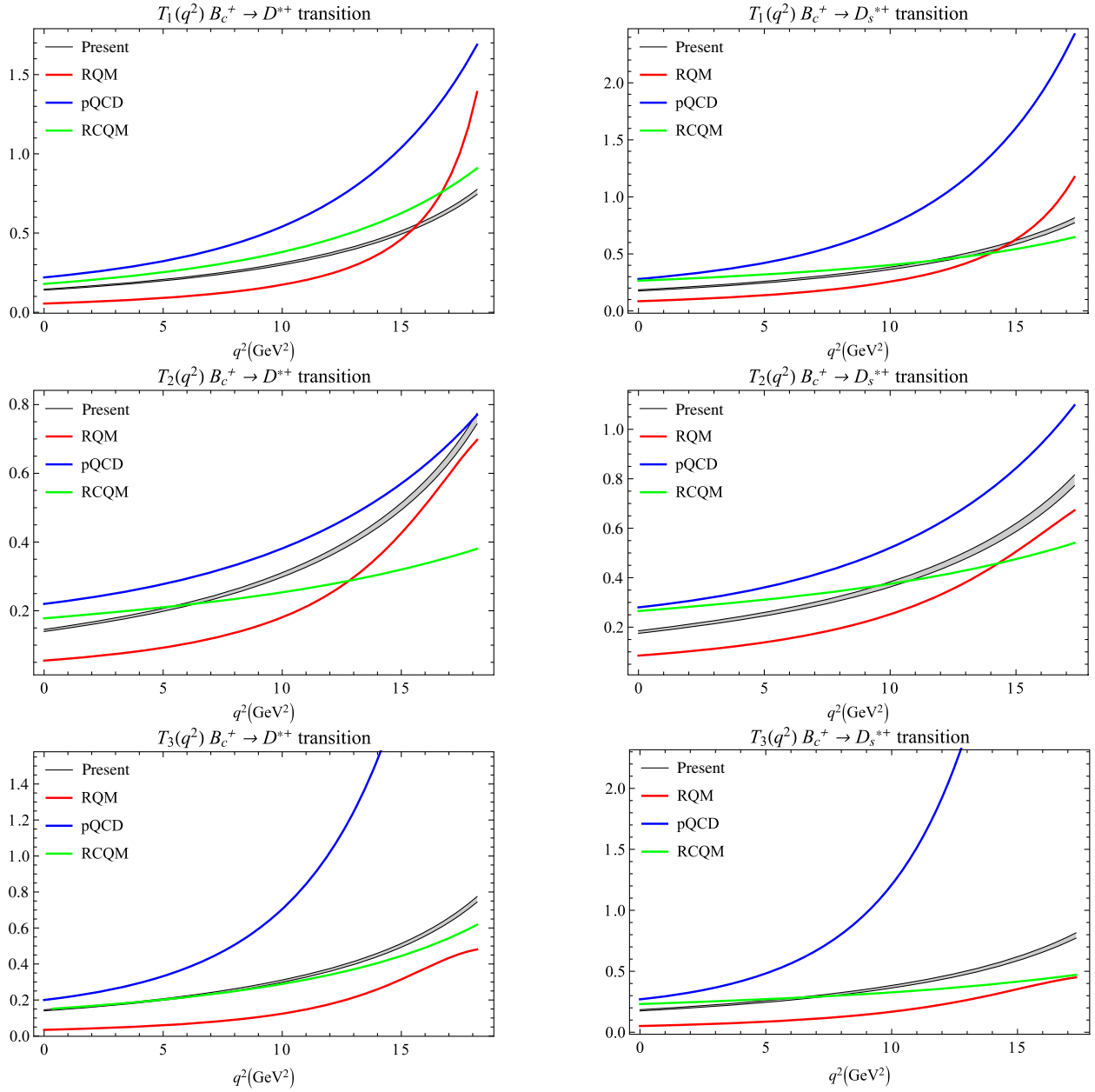

FIG. 5. Form factor comparison for $B_c \to D^*$ (left) and $B_c \to D_s^*$ (right) in comparison with relativistic constituent quark model [49], relativistic quark model [53], perturbative QCD [51], and covariant light front quark model [107].

transition $B_c \to D$ are very similar to the pQCD, LFQM, CQM, and RCQM predictions. Whereas, our results are significantly higher with respect to RQM in almost entire q^2 range. For $B_c \to D_s$ transition also, our results are in good agreement with the LFQM and CQM predictions. Similarly for $B_c \to D^*_{(s)}$ transitions, our form factors are compatible with the RQM and pQCD predictions for the range $q^2 \to q^2_{\mathrm{max}}$, whereas our results are substantially lower for low q^2. The differences in the predictions are mainly attributed to the different methodology employed for the computation of the transition form factors. Using numerical form factors, we have computed branching fractions of rare semileptonic decays using Eq. (17) and in Fig. 6, we plot differential branching fractions. In Table IV, we provide the branching fractions by numerically integrating area under the differential branching fraction curve in Fig. 6. In the differential branching fraction plots, the peaks near to $q^2 = m^2_{J/\psi}$ and $q^2 = m^2_{\psi(2S)}$ correspond to the charm resonances, whereas in the low q^2 range (in the case of $B_c \to D^{(*)}$ transition), they correspond to the light vector resonances appearing in the effective Wilson coefficients. In Table IV, we provide our results considering both with resonance and without resonance contributions. It is important to note here that in

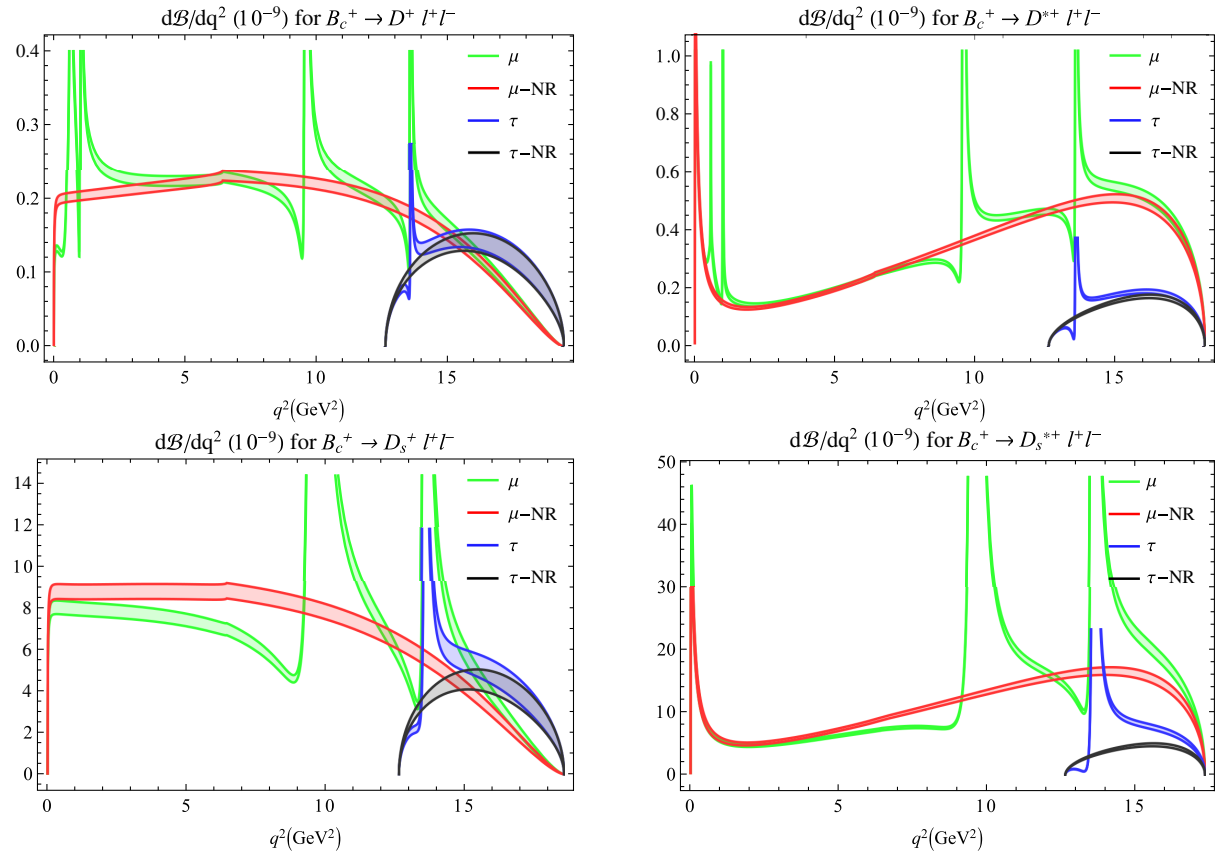

FIG. 6. Differential branching fractions (green and blue plots correspond to the inclusion of vector resonance whereas red and black plots are without the same (NR).).

computations of branching fractions, we exclude the experimentally vetoed q^2 range corresponding to the charm resonances. If we include these range, our results are enhanced by an order of magnitude or more. This is also observed in our recent studies [61] as well as in Ref. [112]. We also compare our results with theoretical predictions from different quark models, perturbative QCD and QCD sum rule approaches. Note that for the transitions corresponding to channels $b \to s\ell^+\ell^-$, we do not include the contribution from the light vector resonances because of the CKM suppression (of the order of λ^2 in Wolfenstein representation); thus we neglect the effects of the second term in effective Hamiltonian equation (1). It is observed that our predictions for the nonresonant branching fractions for some channels are in good agreement with the other theoretical predictions. However, if we include the resonant contributions, our predictions are comparatively lower than the other theoretical approaches. In all the literature mentioned here, the contributions from the light vector resonances are not included for the transition corresponding to $b \to d\ell^+\ell^-$. It is to be noted that for the transitions studied here, experimental data as well as lattice simulation results are not available to the best of our knowledge and understanding, and hence it is not logical to comment on the comparison or credibility of the results from the other theoretical approaches including current study.

In order to explore further effects of leptons in the final state, we study various observables such as forward-backward asymmetry, longitudinal and transverse polarizations, and angular observables using the relations Eqs. (33) and (35). These observables are plotted in the Fig. 7–9 and their expectation values in the whole q^2 range are given in Table V. In these plots, we include the effects of both nonresonant and resonant contributions, where the peaks correspond to charmonia and light vector resonances. We also compute the expectation values of these observables in the different q^2 bins corresponding to the exclusion of contributions from vector resonances. Very recently, Li have studied the branching fractions and other observables for the channel $B_c \to D_s^*\ell^+\ell^-$ in the framework of covariant light front quark model (CLFQM) [107]. The authors have computed the transition form factors using the modified Isgur-Wise function. We compare our results of the observables with CLFQM results in Tables VI–IX and it is observed that many of our results are not in agreement with the CLFQM results. The differences are mainly arising due to their inclusion of the contribution of light vector resonances [107].

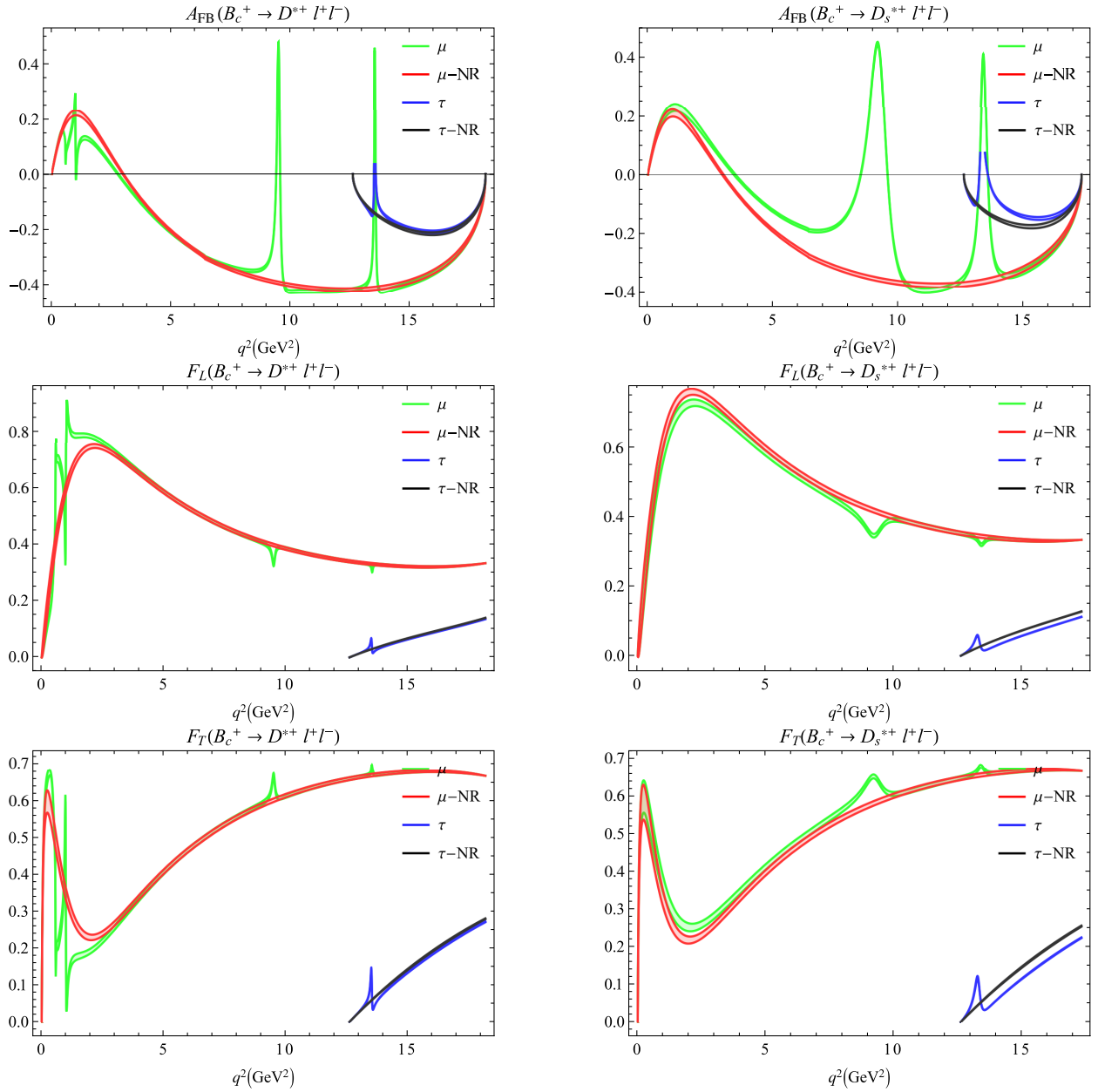

FIG. 7. Forward-backward asymmetry, longitudinal and transverse polarization fractions (Green and Blue plots correspond to the inclusion of vector resonance whereas Red and Black plots are without the same (NR).).

The light vector resonances have been excluded earlier also for the transition corresponding to the quark channel $b \to s\ell^+\ell^-$ employing CCQM [90,110]. To the best of our knowledge and understanding, these observables are yet to be studied using any other theoretical approaches and further these channels are also yet to be explored by the worldwide experimental facilities. These observables are dependent on the lepton flavors and thus serve as very important probe for the search of new physics beyond the standard model and therefore some insights from the very recent run from the LHCb collaborations as well as from other B factories are expected.

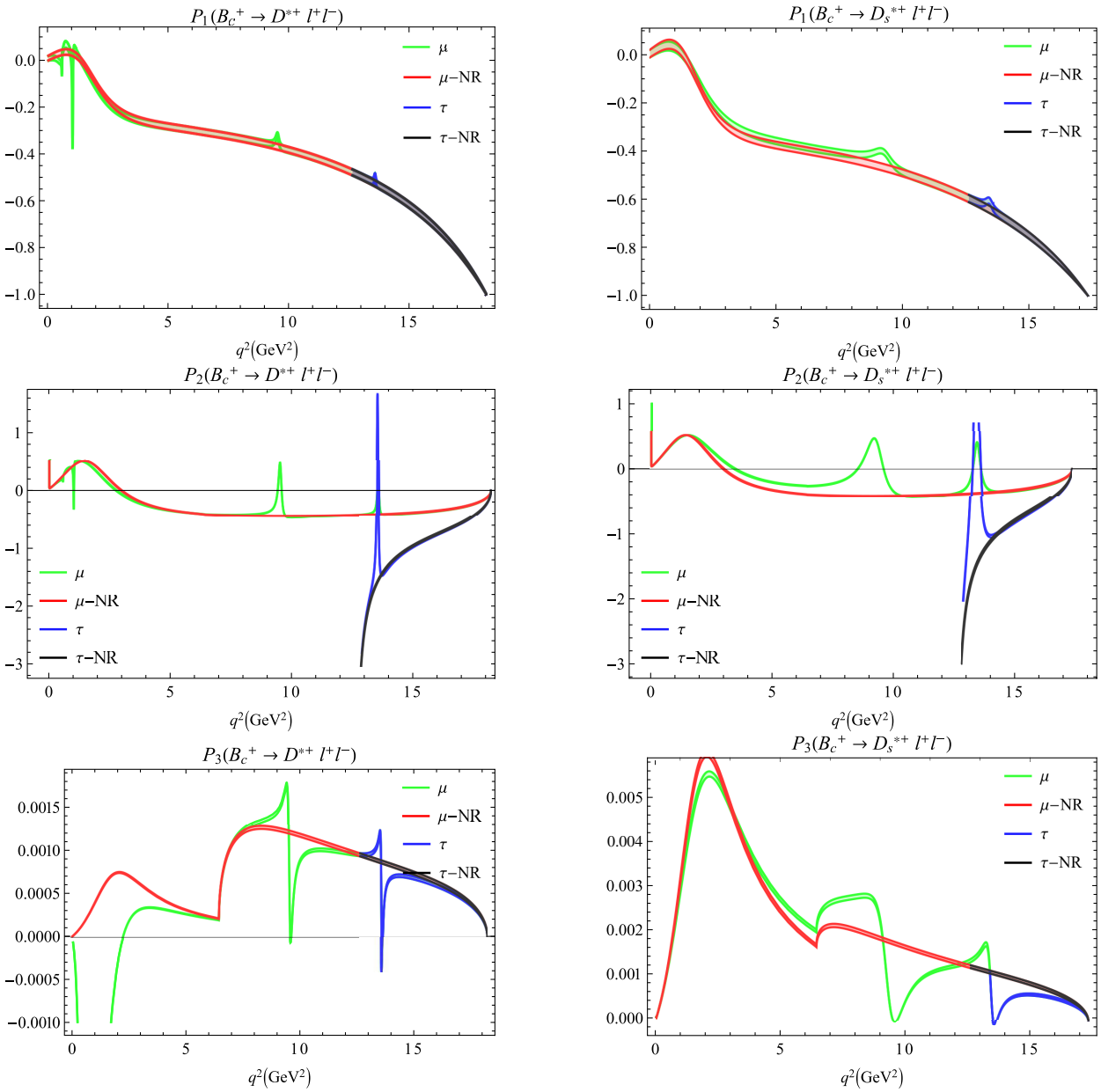

FIG. 8. Clean observables $P_{1,2,3}$ in whole q^2 range (green and blue plots correspond to the inclusion of vector resonance whereas red and black plots are without the same (NR).).

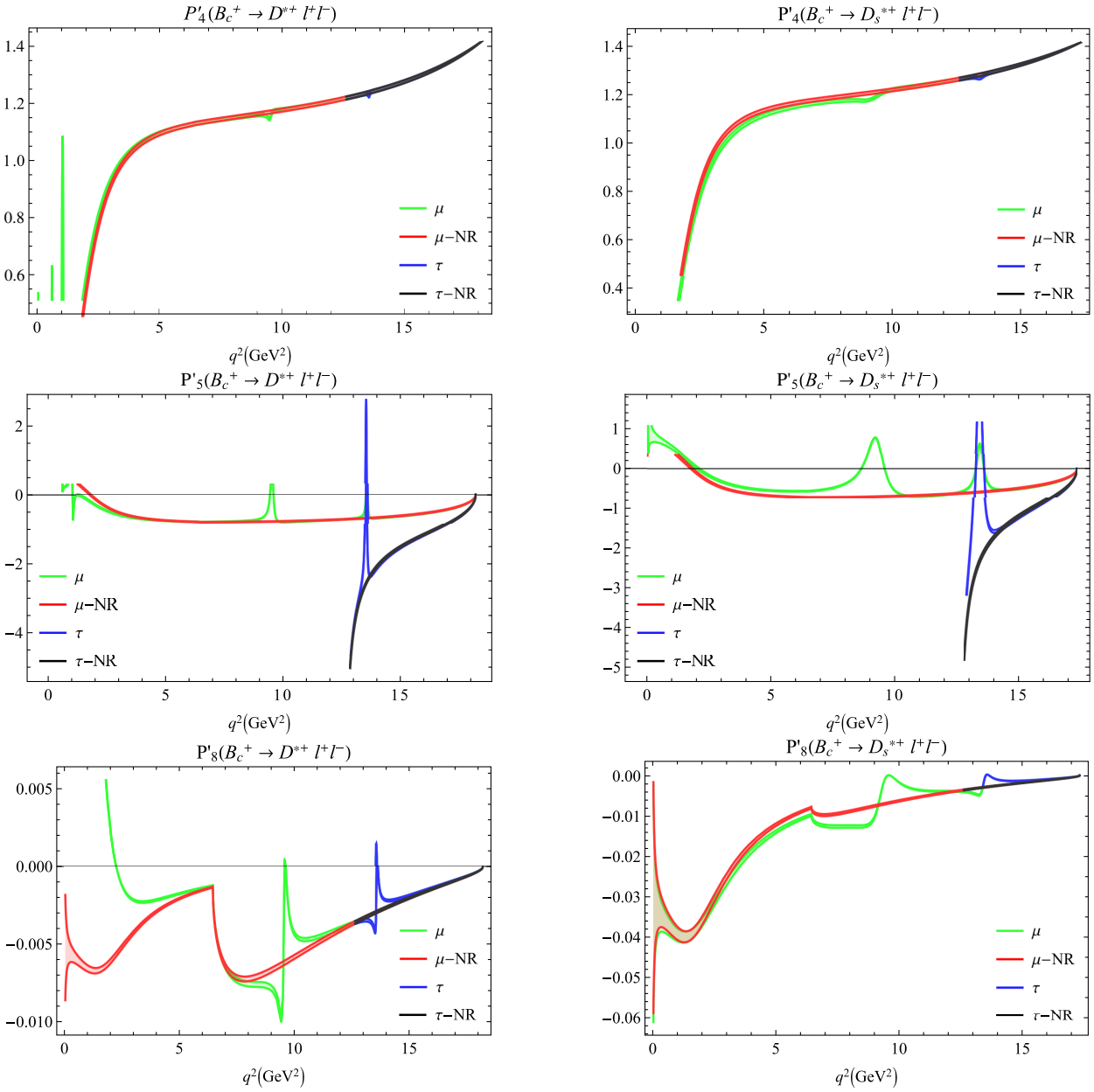

FIG. 9. Clean observables $P_{4,5,8}$ in whole q^2 range (green and blue plots correspond to the inclusion of vector resonance whereas red and black plots are without the same (NR).).

TABLE V. q^2- averages of polarization observables over the whole allowed kinematic region for $B_c^+ \to D^{*+}\ell^+\ell^-$ and $B_c^+ \to D_s^{*+}\ell^+\ell^-$.

Observable	$B_c^+ \to D^{*+}\ell^+\ell^-$			$B_c^+ \to D_s^{*+}\ell^+\ell^-$		
	e^+e^-	$\mu^+\mu^-$	$\tau^+\tau^-$	e^+e^-	$\mu^+\mu^-$	$\tau^+\tau^-$
$-\langle A_{FB}\rangle$	0.805 ± 0.018	0.805 ± 0.018	0.188 ± 0.008	0.657 ± 0.021	0.657 ± 0.021	0.134 ± 0.008
$\langle F_L\rangle$	1.028 ± 0.035	1.215 ± 0.034	0.095 ± 0.005	1.003 ± 0.063	1.199 ± 0.047	0.080 ± 0.006
$\langle F_T\rangle$	1.936 ± 0.040	1.710 ± 0.038	0.200 ± 0.010	1.958 ± 0.063	1.718 ± 0.053	0.163 ± 0.011
$-\langle P_1\rangle$	1.274 ± 0.045	1.403 ± 0.045	0.778 ± 0.041	1.490 ± 0.067	1.644 ± 0.068	0.856 ± 0.062
$-\langle P_2\rangle$	0.819 ± 0.016	0.937 ± 0.017	0.627 ± 0.026	0.676 ± 0.020	0.705 ± 0.021	0.548 ± 0.032
$10^4 \times \langle P_3\rangle$	5.696 ± 0.752	5.255 ± 1.376	4.907 ± 0.464	26.815 ± 0.772	42.481 ± 1.791	4.707 ± 0.221
$\langle P_4'\rangle$	2.992 ± 3.729	3.299 ± 0.082	1.333 ± 0.061	3.005 ± 6.552	3.338 ± 0.116	1.362 ± 0.086
$-\langle P_5'\rangle$	1.428 ± 0.030	1.627 ± 0.032	0.950 ± 0.036	1.112 ± 0.034	1.242 ± 0.037	0.810 ± 0.042
$10^2 \times \langle P_8'\rangle$	3.554 ± 0.194	5.052 ± 0.208	-0.106 ± 0.007	-1.923 ± 0.137	2.491 ± 0.098	0.087 ± 0.008

TABLE VI. Angular observables in bins for the channel $B_c^+ \to D^{*+}$.

Observable	Bin	e^+e^-	$\mu^+\mu^-$	$\tau^+\tau^-$
$\mathcal{B} \times 10^9$	[1.1, 6.0]	0.845 ± 0.026	0.840 ± 0.025	
	[6.0, 8.0]	0.521 ± 0.011	0.519 ± 0.011	
	[11.0, 12.5]	0.681 ± 0.015	0.680 ± 0.015	
	[15.0, 17.0]	1.025 ± 0.032	1.023 ± 0.032	0.367 ± 0.013
$-\langle A_{FB}\rangle$	[1.1, 6.0]	0.087 ± 0.004	0.087 ± 0.004	
	[6.0, 8.0]	0.317 ± 0.009	0.316 ± 0.009	
	[11.0, 12.5]	0.421 ± 0.011	0.421 ± 0.011	
	[15.0, 17.0]	0.353 ± 0.014	0.353 ± 0.014	0.203 ± 0.009
$\langle F_L\rangle$	[1.1, 6.0]	0.685 ± 0.034	0.672 ± 0.034	
	[6.0, 8.0]	0.485 ± 0.019	0.482 ± 0.019	
	[11.0, 12.5]	0.353 ± 0.013	0.352 ± 0.013	
	[15.0, 17.0]	0.321 ± 0.016	0.321 ± 0.016	0.086 ± 0.004
$\langle F_T\rangle$	[1.1, 6.0]	0.315 ± 0.010	0.311 ± 0.010	
	[6.0, 8.0]	0.515 ± 0.013	0.513 ± 0.013	
	[11.0, 12.5]	0.647 ± 0.018	0.645 ± 0.018	
	[15.0, 17.0]	0.679 ± 0.029	0.678 ± 0.029	0.181 ± 0.008

TABLE VII. Same as Table VI.

Observable	Bin	e^+e^-	$\mu^+\mu^-$	$\tau^+\tau^-$
$-\langle P_1\rangle$	[1.1, 6.0]	0.241 ± 0.013	0.242 ± 0.013	
	[6.0, 8.0]	0.315 ± 0.015	0.315 ± 0.015	
	[11.0, 12.5]	0.441 ± 0.019	0.441 ± 0.019	
	[15.0, 17.0]	0.705 ± 0.035	0.705 ± 0.035	0.716 ± 0.036
$-\langle P_2\rangle$	[1.1, 6.0]	0.184 ± 0.008	0.186 ± 0.008	
	[6.0, 8.0]	0.410 ± 0.009	0.412 ± 0.009	
	[11.0, 12.5]	0.434 ± 0.010	0.435 ± 0.010	
	[15.0, 17.0]	0.347 ± 0.013	0.347 ± 0.013	0.746 ± 0.029
$\langle P_3\rangle \times 10^4$	[1.1, 6.0]	$-(0.058 \pm 1.772)$	0.028 ± 1.771	
	[6.0, 8.0]	9.206 ± 0.141	9.209 ± 0.141	
	[11.0, 12.5]	9.752 ± 0.165	9.752 ± 0.165	
	[15.0, 17.0]	5.854 ± 0.169	5.854 ± 0.168	5.730 ± 0.168
$\langle P_4'\rangle$	[1.1, 6.0]	0.878 ± 0.031	0.881 ± 0.031	
	[6.0, 8.0]	1.131 ± 0.034	1.131 ± 0.034	

(Table continued)

TABLE VII. *(Continued)*

Observable	Bin	e^+e^-	$\mu^+\mu^-$	$\tau^+\tau^-$
	[11.0, 12.5]	1.199 ± 0.038	1.199 ± 0.038	
	[15.0, 17.0]	1.306 ± 0.056	1.306 ± 0.056	1.310 ± 0.057
$-\langle P_5' \rangle$	[1.1, 6.0]	0.570 ± 0.022	0.576 ± 0.022	
	[6.0, 8.0]	0.770 ± 0.021	0.772 ± 0.021	
	[11.0, 12.5]	0.731 ± 0.020	0.732 ± 0.020	
	[15.0, 17.0]	0.533 ± 0.019	0.533 ± 0.019	1.144 ± 0.041
$\langle P_8' \rangle \times 10^{-3}$	[1.1, 6.0]	1.695 ± 0.455	1.592 ± 0.453	
	[6.0, 8.0]	$-(5.412 \pm 0.242)$	$-(5.414 \pm 0.242)$	
	[11.0, 12.5]	$-(4.106 \pm 0.134)$	$-(4.106 \pm 0.134)$	
	[15.0, 17.0]	$-(1.385 \pm 0.085)$	$-(1.385 \pm 0.085)$	$-(1.327 \pm 0.084)$

TABLE VIII. Angular observables in bins for the channel $B_c^+ \to D_s^{*+}$.

Observable	Bin	e^+e^-	[107]	$\mu^+\mu^-$	[107]	$\tau^+\tau^-$	[107]
$10^9 \times \mathcal{B}$	[1.1, 6.0]	26.998 ± 0.917	6.240	26.827 ± 0.915	6.220		
	[6.0, 8.0]	14.930 ± 0.376	3.560	14.854 ± 0.375	3.550		
	[11.0, 12.5]	25.582 ± 0.754	2.830	25.518 ± 0.752	2.830		
	[15.0, 17.0]	34.543 ± 1.647	2.560	34.478 ± 1.644	2.560	13.483 ± 0.685	0.980
$-\langle A_{FB} \rangle$	[1.1, 6.0]	0.002 ± 0.004	0.061	0.003 ± 0.004	0.061		
	[6.0, 8.0]	0.178 ± 0.007	0.243	0.178 ± 0.007	0.242		
	[11.0, 12.5]	0.386 ± 0.014	0.340	0.385 ± 0.014	0.339		
	[15.0, 17.0]	0.270 ± 0.016	0.254	0.270 ± 0.016	0.254	0.138 ± 0.009	0.143
$\langle F_L \rangle$	[1.1, 6.0]	0.651 ± 0.038	0.815	0.640 ± 0.037	0.817		
	[6.0, 8.0]	0.483 ± 0.021	0.637	0.481 ± 0.022	0.638		
	[11.0, 12.5]	0.366 ± 0.019	0.446	0.365 ± 0.018	0.446		
	[15.0, 17.0]	0.331 ± 0.024	0.352	0.330 ± 0.024	0.352	0.079 ± 0.006	0.410
$\langle F_T \rangle$	[1.1, 6.0]	0.349 ± 0.013	0.185	0.344 ± 0.013	0.183		
	[6.0, 8.0]	0.517 ± 0.015	0.363	0.515 ± 0.015	0.362		
	[11.0, 12.5]	0.634 ± 0.024	0.554	0.632 ± 0.024	0.554		
	[15.0, 17.0]	0.669 ± 0.044	0.648	0.667 ± 0.044	0.648	0.159 ± 0.011	0.590

TABLE IX. Same as Table VIII.

Observable	Bin	e^+e^-	[107]	$\mu^+\mu^-$	[107]	$\tau^+\tau^-$	[107]
$-\langle P_1 \rangle$	[1.1, 6.0]	0.282 ± 0.015	0.281	0.284 ± 0.015	0.281		
	[6.0, 8.0]	0.399 ± 0.017	0.408	0.399 ± 0.017	0.408		
	[11.0, 12.5]	0.557 ± 0.027	0.543	0.557 ± 0.027	0.543		
	[15.0, 17.0]	0.834 ± 0.059	0.822	0.834 ± 0.059	0.822	0.845 ± 0.060	0.826
$-\langle P_2 \rangle$	[1.1, 6.0]	0.003 ± 0.008	0.125	0.005 ± 0.008	0.125		
	[6.0, 8.0]	0.229 ± 0.008	0.446	0.230 ± 0.008	0.446		
	[11.0, 12.5]	0.406 ± 0.013	0.409	0.406 ± 0.013	0.409		
	[15.0, 17.0]	0.269 ± 0.059	0.262	0.270 ± 0.015	0.262	0.579 ± 0.034	0.269
$10^4 \times \langle P_3 \rangle$	[1.1, 6.0]	35.666 ± 2.953	1.840	35.587 ± 2.947	1.840		
	[6.0, 8.0]	25.421 ± 1.062	0.070	25.423 ± 1.061	0.070		
	[11.0, 12.5]	12.046 ± 0.288	24.210	12.047 ± 0.288	24.210		
	[15.0, 17.0]	5.114 ± 0.230	34.420	5.113 ± 0.230	34.420	4.944 ± 0.228	20.080
$\langle P_4' \rangle$	[1.1, 6.0]	0.882 ± 0.037	0.908	0.885 ± 0.037	0.898		
	[6.0, 8.0]	1.160 ± 0.040	1.177	1.160 ± 0.040	1.169		
	[11.0, 12.5]	1.247 ± 0.052	1.240	1.247 ± 0.052	1.236		
	[15.0, 17.0]	1.354 ± 0.084	1.350	1.354 ± 0.084	1.347	1.358 ± 0.085	0.561

(Table continued)

TABLE IX. *(Continued)*

Observable	Bin	e^+e^-	[107]	$\mu^+\mu^-$	[107]	$\tau^+\tau^-$	[107]
$-\langle P_5' \rangle$	[1.1, 6.0]	0.315 ± 0.023	0.540	0.319 ± 0.023	0.534		
	[6.0, 8.0]	0.507 ± 0.019	0.766	0.508 ± 0.019	0.761		
	[11.0, 12.5]	0.654 ± 0.023	0.664	0.656 ± 0.023	0.662		
	[15.0, 17.0]	0.399 ± 0.020	0.390	0.399 ± 0.020	0.390	0.855 ± 0.044	0.163
$-10^3 \times \langle P_8' \rangle$	[1.1, 6.0]	22.160 ± 0.980	1.196	22.052 ± 0.975	1.164		
	[6.0, 8.0]	11.841 ± 0.473	0.029	11.842 ± 0.473	0.029		
	[11.0, 12.5]	3.866 ± 0.206	7.054	3.866 ± 0.206	7.030		
	[15.0, 17.0]	0.970 ± 0.088	6.147	0.970 ± 0.088	6.137	0.921 ± 0.085	1.467

V. SUMMARY AND CONCLUSION

In this article, we systematically study the rare semileptonic decay of B_c meson within the framework of covariant confined quark model. We have considered the channels $B_c^+ \to D^{+(*)}\ell^+\ell^-$ and $B_c^+ \to D_s^{+(*)}\ell^+\ell^-$ for all the lepton flavors. The necessary transition form factors are computed in the whole range of momentum transfer squared and compared with different theoretical approaches. Our results of the form factors are compatible with the other quark models. Using these form factors and Wilson coefficients, we have computed the rare semileptonic branching fractions and compared our results with other approaches. We have also computed various observables such as forward-backward asymmetry, longitudinal and transverse polarizations, and angular observables. In present work, the computation of effective Wilson coefficients includes the contribution of charm resonances as well as light vector resonances in the case of $B_c^+ \to D^{+(*)}\ell^+\ell^-$. For $B_c^+ \to D_s^{+(*)}\ell^+\ell^-$, we only include the contribution of charm vector resonances. It is observed that our predictions are systematically lower than those reported in literature and the main reason for these differences are the inclusion of the contribution of light vector resonances in definition of effective Wilson coefficients as well as the choice of the numerical values of the Wilson coefficients.

To conclude, we have provided the complete description of rare semileptonic decays of B_c mesons in the framework of CCQM along with the different physical observables which would play an important role for the identification of these observables for future experimental facilities and also to look for the test of new physics beyond standard model, if any.

ACKNOWLEDGMENTS

N. R. S. would like to thank INFN (Napoli Section) for the postdoctoral research grant (Assegno di ricerca) No. 24496/2022.

APPENDIX: COVARIANCE AMONG FORM FACTOR PARAMETERS

Within the framework of CCQM, the theoretical uncertainties are directly tied to the uncertainties in the free parameters of the model. To provide the reader with a practical way to utilise our model, we fit the behavior of the form factors as a function of q^2 using

TABLE X. Covariance matrix for $B_c^+ \to D^+$ form factors and associated parameters ($\times 10^{-3}$).

		F_+			F_-			F_T			F_0		
		$F(0)$	a	b	$F(0)$	a	b	$F(0)$	a	b	$F(0)$	a	b
F_+	$F(0)$	0.009	0.036	0.081	−0.006	0.033	0.078	0.012	0.036	0.084	0.012	0.135	0.336
	a		0.144	0.324	−0.024	0.132	0.312	0.048	0.144	0.336	0.048	0.540	1.344
	b			0.729	−0.054	0.297	0.702	0.108	0.324	0.756	0.108	1.215	3.024
F_-	$F(0)$				0.004	−0.022	−0.052	−0.008	−0.024	−0.056	−0.008	−0.090	−0.224
	a					0.121	0.286	0.044	0.132	0.308	0.044	0.495	1.232
	b						0.676	0.104	0.312	0.728	0.104	1.170	2.912
F_T	$F(0)$							0.016	0.048	0.112	0.016	0.180	0.448
	a								0.144	0.336	0.048	0.540	1.344
	b									0.784	0.112	1.260	3.136
F_0	$F(0)$										0.016	0.180	0.448
	a											2.025	5.040
	b												12.544

TABLE XI. Covariance matrix for $B_c^+ \to D_s^+$ form factors and associated parameters ($\times 10^{-3}$).

		F_+			F_-			F_T			F_0		
		$F(0)$	a	b	$F(0)$	a	b	$F(0)$	a	b	$F(0)$	a	b
F_+	$F(0)$	0.016	−0.076	−0.184	−0.016	0.038	−0.180	−0.024	−0.076	0.188	−0.024	−0.228	−0.596
	a		0.361	0.874	0.076	−0.180	0.855	0.114	0.361	−0.893	0.114	1.083	2.831
	b			2.116	0.184	−0.437	2.070	0.276	0.874	−2.162	0.276	2.622	6.853
F_-	$F(0)$				0.016	−0.038	0.180	0.024	0.076	−0.188	0.024	0.228	0.596
	a					0.361	−0.427	−0.057	−0.180	0.446	−0.057	−0.541	−1.415
	b						2.025	0.270	0.855	−2.115	0.270	2.565	6.705
F_T	$F(0)$							0.036	0.114	−0.282	0.036	0.342	0.894
	a								0.361	−0.893	0.114	1.083	2.831
	b									2.209	−0.282	−2.679	−7.003
F_0	$F(0)$										0.036	0.342	0.894
	a											3.249	8.493
	b												22.201

the double-pole parametrization which is characterized by three parameters [namely $F(0)$, a and b], has been fitted using a standard chi-squared minimization procedure. Here, we present the covariance matrices for all the transition form factors for the channels $B_c^+ \to D_{(s)}^+$ as well as for the channels $B_c^+ \to D_{(s)}^{*+}$. They demonstrate the covariance among the parameters corresponding to all form factors entering the same decay channel. All the matrices are listed in Tables X–XIII.

TABLE XII. Covariance matrix for $B_c^+ \to D^{*+}$ form factors and associated parameters ($\times 10^{-3}$).

		A_0			A_+			A_-			V			a_0			a_+			g	
		$F(0)$	a	b	$F(0)$	a	b	$F(0)$	a	b	$F(0)$	a	b	$F(0)$	a	b	$F(0)$	a	b	$F(0)$	a	b
A_0	$F(0)$	0.004	0.020	0.052	0.002	−0.014	−0.034	−0.004	−0.012	−0.030	0.004	−0.012	−0.030	−0.002	−0.020	−0.050	−0.018	−0.014	−0.036	−0.002	−0.012	−0.028
	a		0.100	0.260	0.010	−0.070	−0.170	−0.020	−0.060	−0.150	0.020	−0.060	−0.150	−0.010	−0.100	−0.250	−0.090	−0.070	−0.180	−0.010	−0.060	−0.140
	b			0.676	0.026	−0.182	−0.442	−0.052	−0.156	−0.390	0.052	−0.156	−0.390	−0.026	−0.260	−0.650	−0.234	−0.182	−0.468	−0.026	−0.156	−0.364
A_+	$F(0)$				0.001	−0.007	−0.017	−0.002	−0.006	−0.015	0.002	−0.006	−0.015	−0.001	−0.010	−0.025	−0.009	−0.007	−0.018	−0.001	−0.006	−0.014
	a					0.049	0.119	0.014	0.042	0.105	−0.014	0.042	0.105	0.007	0.070	0.175	0.063	0.049	0.126	0.007	0.042	0.098
	b						0.289	0.034	0.102	0.255	−0.034	0.102	0.255	0.017	0.170	0.425	0.153	0.119	0.306	17.000	0.102	0.238
A_-	$F(0)$							0.004	0.012	0.030	−0.004	0.012	0.030	0.002	0.020	0.050	0.002	0.020	0.050	0.002	0.012	0.028
	a								0.036	0.090	−0.012	0.036	0.090	0.006	0.060	0.150	0.054	0.042	0.108	0.006	0.036	0.084
	b									0.225	−0.030	0.090	0.225	0.015	0.150	0.375	0.135	0.105	0.270	0.015	0.090	0.210
V	$F(0)$										0.004	−0.012	−0.030	−0.002	−0.020	−0.050	−0.018	−0.014	−0.036	−0.002	−0.012	−0.028
	a											0.036	0.090	0.006	0.060	0.140	0.054	0.042	0.108	0.006	0.036	0.084
	b												0.225	0.015	0.150	0.375	0.135	0.105	0.270	0.015	0.090	0.210
a_0	$F(0)$													0.001	0.010	0.025	0.009	0.007	0.018	0.001	0.006	0.014
	a														0.100	0.250	0.090	0.070	0.180	0.010	0.060	0.140
	b															0.625	0.225	0.175	0.450	0.025	0.150	0.350
a_+	$F(0)$																0.081	0.063	0.162	0.009	0.054	0.126
	a																	0.049	0.126	0.007	0.042	0.098
	b																		0.324	0.018	0.108	0.252
g	$F(0)$																			0.001	0.006	0.014
	a																				0.036	0.084
	b																					0.196

TABLE XIII. Covariance matrix for $B_c^+ \to D_s^{*+}$ form factors and associated parameters ($\times 10^{-3}$).

		A_0			A_+			A_-			V			a_0			a_+			g	
		$F(0)$	a	b	$F(0)$	a	b	$F(0)$	a	b	$F(0)$	a	b	$F(0)$	a	b	$F(0)$	a	b	$F(0)$	a	b
A_0	$F(0)$	0.009	0.048	0.123	0.006	−0.033	−0.087	−0.009	−0.030	−0.078	0.006	−0.030	−0.078	−0.006	−0.045	−0.117	−0.006	−0.033	−0.087	−0.006	−0.030	−0.075
	a		0.256	0.656	0.032	−0.176	−0.464	−0.048	−0.160	−0.416	0.032	−0.160	−0.416	−0.032	−0.240	−0.624	−0.032	−0.176	−0.464	−0.032	−0.160	−0.400
	b			1.681	0.082	−0.451	−1.189	−0.123	−0.410	−1.066	0.082	−0.410	−1.066	−0.082	−0.615	−1.599	−0.082	−0.451	−1.189	−0.082	−0.410	−1.025
A_+	$F(0)$				0.004	−0.022	−0.058	−0.006	−0.020	−0.052	0.004	−0.020	−0.052	−0.004	−0.030	−0.078	−0.004	−0.022	−0.058	−0.004	−0.020	−0.050
	a					0.121	0.319	0.033	0.110	0.286	−0.022	0.110	0.286	0.022	0.165	0.429	0.022	0.121	0.319	0.022	0.110	0.275
	b						0.841	0.087	0.29	0.754	−0.058	0.290	0.754	0.058	0.435	1.131	0.058	0.319	0.841	0.058	0.290	0.725
A_-	$F(0)$							0.009	0.030	0.078	−0.006	0.030	0.078	0.006	0.045	0.117	0.006	0.045	0.117	0.006	0.030	0.075
	a								0.100	0.260	−0.020	0.100	0.260	0.020	0.150	0.390	0.020	0.110	0.290	0.020	0.100	0.250
	b									0.676	−0.052	0.260	0.676	0.052	0.390	1.014	0.052	0.286	0.754	0.052	0.260	0.650
V	$F(0)$										0.004	−0.020	−0.052	−0.004	−0.030	−0.078	−0.004	−0.022	−0.058	−0.004	−0.020	−0.050
	a											0.100	0.260	0.020	0.150	0.390	0.020	0.110	0.290	0.020	0.100	0.250
	b												0.676	0.052	0.390	1.014	0.052	0.286	0.754	0.052	0.260	0.650
a_0	$F(0)$													0.004	0.030	0.078	0.004	0.022	0.058	0.004	0.020	0.050
	a														0.225	0.585	0.030	0.165	0.435	0.030	0.150	0.375
	b															1.521	0.078	0.429	1.131	0.078	0.390	0.975
a_+	$F(0)$																0.004	0.022	0.058	0.004	0.020	0.050
	a																	0.121	0.319	0.022	0.110	0.275
	b																		0.841	0.058	0.290	0.725
g	$F(0)$																			0.004	0.020	0.050
	a																				0.100	0.250
	b																					0.625

[1] J. P. Lees *et al.* (*BABAR* Collaboration), Phys. Rev. D **88**, 072012 (2013).
[2] M. Huschle *et al.* (Belle Collaboration), Phys. Rev. D **92**, 072014 (2015).
[3] Y. Sato *et al.* (Belle Collaboration), Phys. Rev. D **94**, 072007 (2016).
[4] R. Aaij *et al.* (LHCb Collaboration), Phys. Rev. Lett. **115**, 111803 (2015); **115**, 159901(E) (2015).
[5] R. Aaij *et al.* (LHCb Collaboration), Phys. Rev. Lett. **120**, 171802 (2018).
[6] R. Aaij *et al.* (LHCb Collaboration), Phys. Rev. Lett. **131**, 111802 (2023).
[7] A. Mathad (LHCb Collaboration), arXiv:2305.08133.
[8] R. Aaij *et al.* (LHCb Collaboration), Phys. Rev. Lett. **120**, 121801 (2018).
[9] J. Harrison, C. T. H. Davies, and A. Lytle (LATTICE-HPQCD Collaboration), Phys. Rev. Lett. **125**, 222003 (2020).
[10] A. Di Canto and S. Meinel, arXiv:2208.05403.
[11] A. Crivellin and J. Matias, arXiv:2204.12175.
[12] A. J. Bevan *et al.* (*BABAR* and Belle Collaborations), Eur. Phys. J. C **74**, 3026 (2014).
[13] CMS Collaboration, Rep. Prog. Phys. **87**, 077802 (2024).
[14] R. Aaij *et al.* (LHCb Collaboration), Phys. Rev. Lett. **131**, 051803 (2023).
[15] R. Aaij *et al.* (LHCb Collaboration), Nat. Phys. **18**, 277 (2022); **19**, 1517(E) (2023).
[16] R. Aaij *et al.* (LHCb Collaboration), Phys. Rev. Lett. **128**, 191802 (2022).
[17] A. Abdesselam *et al.* (Belle Collaboration), Phys. Rev. Lett. **126**, 161801 (2021).
[18] S. Choudhury *et al.* (Belle Collaboration), J. High Energy Phys. 03 (2021) 105.
[19] R. Aaij *et al.* (LHCb Collaboration), Phys. Rev. Lett. **125**, 011802 (2020).
[20] R. Aaij *et al.* (LHCb Collaboration), Phys. Rev. Lett. **122**, 191801 (2019).
[21] R. Aaij *et al.* (LHCb Collaboration), J. High Energy Phys. 08 (2017) 055.
[22] R. Aaij *et al.* (LHCb Collaboration), J. High Energy Phys. 02 (2016) 104.
[23] R. Aaij *et al.* (LHCb Collaboration), Phys. Rev. Lett. **113**, 151601 (2014).
[24] R. Aaij *et al.* (LHCb Collaboration), Phys. Rev. Lett. **111**, 191801 (2013).
[25] J. P. Lees *et al.* (*BABAR* Collaboration), Phys. Rev. Lett. **118**, 031802 (2017).
[26] J. P. Lees *et al.* (*BABAR* Collaboration), Phys. Rev. D **86**, 032012 (2012).
[27] N. Gubernari, D. van Dyk, and J. Virto, J. High Energy Phys. 02 (2021) 088.
[28] A. Khodjamirian, T. Mannel, A. A. Pivovarov, and Y. M. Wang, J. High Energy Phys. 09 (2010) 089.
[29] M. Bordone, G. isidori, S. Mächler, and A. Tinari, Eur. Phys. J. C **84**, 547 (2024).
[30] M. Algueró, A. Biswas, B. Capdevila, S. Descotes-Genon, J. Matias, and M. Novoa-Brunet, Eur. Phys. J. C **83**, 648 (2023).
[31] N. Gubernari, M. Reboud, D. van Dyk, and J. Virto, J. High Energy Phys. 09 (2022) 133.
[32] T. Hurth, F. Mahmoudi, and S. Neshatpour, Phys. Rev. D **103**, 095020 (2021).
[33] M. Ciuchini, A. M. Coutinho, M. Fedele, E. Franco, A. Paul, L. Silvestrini, and M. Valli, Eur. Phys. J. C **79**, 719 (2019).
[34] M. Algueró, B. Capdevila, S. Descotes-Genon, P. Masjuan, and J. Matias, Phys. Rev. D **99**, 075017 (2019).
[35] S. Descotes-Genon, L. Hofer, J. Matias, and J. Virto, J. High Energy Phys. 12 (2014) 125.
[36] A. Seuthe (LHCb Collaboration), arXiv:2305.08216.
[37] R. Aaij *et al.* (LHCb Collaboration), Phys. Rev. D **108**, 032002 (2023).
[38] I. Adachi *et al.* (Belle-II and Belle Collaborations), Phys. Rev. Lett. **133**, 101804 (2024).
[39] R. Aaij *et al.* (LHCb Collaboration), J. High Energy Phys. 04 (2017) 029.
[40] R. Aaij *et al.* (LHCb Collaboration), J. High Energy Phys. 10 (2015) 034.
[41] R. Aaij *et al.* (LHCb Collaboration), J. High Energy Phys. 12 (2012) 125.
[42] R. Aaij *et al.* (LHCb Collaboration), J. High Energy Phys. 07 (2018) 020.
[43] M. Artuso, G. Isidori, and S. Stone, *New Physics in B Decays* (World Scientific, Singapore, 2022).
[44] D. London and J. Matias, Annu. Rev. Nucl. Part. Sci. **72**, 37 (2022).
[45] R. Aaij *et al.* (LHCb Collaboration), J. High Energy Phys. 02 (2024) 032.
[46] C. Q. Geng, C.-W. Hwang, and C. C. Liu, Phys. Rev. D **65**, 094037 (2002).
[47] K. Azizi, F. Falahati, V. Bashiry, and S. M. Zebarjad, Phys. Rev. D **77**, 114024 (2008).
[48] K. Azizi and R. Khosravi, Phys. Rev. D **78**, 036005 (2008).
[49] A. Faessler, T. Gutsche, M. A. Ivanov, J. G. Korner, and V. E. Lyubovitskij, Eur. Phys. J. direct C **4**, 18 (2002).
[50] H.-M. Choi, Phys. Rev. D **81**, 054003 (2010).
[51] W.-F. Wang, X. Yu, C.-D. Lü, and Z.-J. Xiao, Phys. Rev. D **90**, 094018 (2014).
[52] U. O. Yilmaz, Phys. Rev. D **85**, 115026 (2012).
[53] D. Ebert, R. N. Faustov, and V. O. Galkin, Phys. Rev. D **82**, 034032 (2010).
[54] P. Maji, S. Mahata, P. Nayek, S. Biswas, and S. Sahoo, Chin. Phys. C **44**, 073106 (2020).
[55] P. Maji, S. Biswas, P. Nayek, and S. Sahoo, Prog. Theor. Exp. Phys. **2020**, 053B07 (2020).
[56] R. Dutta, Phys. Rev. D **100**, 075025 (2019).
[57] M. K. Mohapatra, N. Rajeev, and R. Dutta, Phys. Rev. D **105**, 115022 (2022).
[58] M. Zaki, M. A. Paracha, and F. M. Bhutta, Nucl. Phys. **B992**, 116236 (2023).
[59] J. N. Pandya, P. Santorelli, and N. R. Soni, arXiv:2307.14245.
[60] N. R. Soni, A. Issadykov, A. N. Gadaria, Z. Tyulemissov, J. J. Patel, and J. N. Pandya, Eur. Phys. J. Plus **138**, 163 (2023).
[61] N. R. Soni, A. Issadykov, A. N. Gadaria, J. J. Patel, and J. N. Pandya, Eur. Phys. J. A **58**, 39 (2022).
[62] N. R. Soni, A. N. Gadaria, J. J. Patel, and J. N. Pandya, Phys. Rev. D **102**, 016013 (2020).

[63] M. A. Ivanov, J. G. Körner, J. N. Pandya, P. Santorelli, N. R. Soni, and C.-T. Tran, Front. Phys. (Beijing) **14**, 64401 (2019).
[64] N. R. Soni, M. A. Ivanov, J. G. Körner, J. N. Pandya, P. Santorelli, and C. T. Tran, Phys. Rev. D **98**, 114031 (2018).
[65] N. R. Soni and J. N. Pandya, Phys. Rev. D **96**, 016017 (2017); **99**, 059901(E) (2019).
[66] A. J. Buras and M. Munz, Phys. Rev. D **52**, 186 (1995).
[67] F. Kruger and L. Sehgal, Phys. Rev. D **55**, 2799 (1997).
[68] G. Buchalla, A. J. Buras, and M. E. Lautenbacher, Rev. Mod. Phys. **68**, 1125 (1996).
[69] N. Deshpande, J. Trampetic, and K. Panose, Phys. Rev. D **39**, 1461 (1989).
[70] M. Jezabek and J. H. Kuhn, Nucl. Phys. **B320**, 20 (1989).
[71] C. Lim, T. Morozumi, and A. Sanda, Phys. Lett. B **218**, 343 (1989).
[72] M. Misiak, Nucl. Phys. **B393**, 23 (1993); **B439**, 461(E) (1995).
[73] P. J. O'Donnell and H. K. Tung, Phys. Rev. D **43**, R2067 (1991).
[74] A. Ali, T. Mannel, and T. Morozumi, Phys. Lett. B **273**, 505 (1991).
[75] C. Bobeth, M. Misiak, and J. Urban, Nucl. Phys. **B574**, 291 (2000).
[76] C.-H. Chen and C. Q. Geng, Phys. Rev. D **64**, 074001 (2001).
[77] W.-F. Wang and Z.-J. Xiao, Phys. Rev. D **86**, 114025 (2012).
[78] S. Navas *et al.* (Particle Data Group), Phys. Rev. D **110**, 030001 (2024).
[79] S. Descotes-Genon, T. Hurth, J. Matias, and J. Virto, J. High Energy Phys. 05 (2013) 137.
[80] G. V. Efimov and M. A. Ivanov, Int. J. Mod. Phys. A **04**, 2031 (1989).
[81] G. V. Efimov and M. A. Ivanov, *The Quark Confinement Model of Hadrons* (IOP, Bristol, 1993).
[82] M. A. Ivanov and P. Santorelli, Phys. Lett. B **456**, 248 (1999).
[83] T. Branz, A. Faessler, T. Gutsche, M. A. Ivanov, J. G. Korner, and V. E. Lyubovitskij, Phys. Rev. D **81**, 034010 (2010).
[84] M. A. Ivanov, J. G. Korner, S. G. Kovalenko, P. Santorelli, and G. G. Saidullaeva, Phys. Rev. D **85**, 034004 (2012).
[85] T. Gutsche, M. A. Ivanov, J. G. Korner, V. E. Lyubovitskij, and P. Santorelli, Phys. Rev. D **86**, 074013 (2012).
[86] A. Salam, Nuovo Cimento **25**, 224 (1962).
[87] S. Weinberg, Phys. Rev. **130**, 776 (1963).
[88] M. A. Ivanov, J. G. Körner, and C. T. Tran, Phys. Rev. D **92**, 114022 (2015).
[89] G. Ganbold, T. Gutsche, M. A. Ivanov, and V. E. Lyubovitskij, J. Phys. G **42**, 075002 (2015).
[90] S. Dubnička, A. Z. Dubničková, A. Issadykov, M. A. Ivanov, A. Liptaj, and S. K. Sakhiyev, Phys. Rev. D **93**, 094022 (2016).
[91] F. James and M. Roos, Comput. Phys. Commun. **10**, 343 (1975).
[92] G. Buchalla and A. J. Buras, Nucl. Phys. **B548**, 309 (1999).
[93] M. Misiak and J. Urban, Phys. Lett. B **451**, 161 (1999).
[94] J. Brod, M. Gorbahn, and E. Stamou, Phys. Rev. D **83**, 034030 (2011).
[95] A. Issadykov and M. A. Ivanov, Mod. Phys. Lett. A **38**, 2350006 (2023).
[96] R. Aaij *et al.* (LHCb Collaboration), J. High Energy Phys. 02 (2016) 104.
[97] S. Wehle *et al.* (Belle Collaboration), Phys. Rev. Lett. **118**, 111801 (2017).
[98] R. Aaij *et al.* (LHCb Collaboration), J. High Energy Phys. 09 (2015) 179.
[99] R. Aaij *et al.* (LHCb Collaboration), J. High Energy Phys. 09 (2018) 146.
[100] A. Arbey, T. Hurth, F. Mahmoudi, D. Martínez Santos, and S. Neshatpour, Phys. Rev. D **100**, 015045 (2019).
[101] K. Kowalska, D. Kumar, and E. M. Sessolo, Eur. Phys. J. C **79**, 840 (2019).
[102] A. K. Alok, A. Dighe, S. Gangal, and D. Kumar, J. High Energy Phys. 06 (2019) 089.
[103] G. Hiller and M. Schmaltz, Phys. Rev. D **90**, 054014 (2014).
[104] G. Hiller, D. Loose, Nis, and I. Zic, Phys. Rev. D **97**, 075004 (2018).
[105] A. Crivellin, D. Müller, and T. Ota, J. High Energy Phys. 09 (2017) 040.
[106] P. Ko, Y. Omura, Y. Shigekami, and C. Yu, Phys. Rev. D **95**, 115040 (2017).
[107] Y.-S. Li and X. Liu, Phys. Rev. D **108**, 093005 (2023).
[108] B. Kindra and N. Mahajan, Phys. Rev. D **98**, 094012 (2018).
[109] J. Matias, Phys. Rev. D **86**, 094024 (2012).
[110] S. Dubnička, A. Z. Dubničková, N. Habyl, M. A. Ivanov, A. Liptaj, and G. S. Nurbakova, Few-Body Syst. **57**, 121 (2016).
[111] M. Wirbel, B. Stech, and M. Bauer, Z. Phys. C **29**, 637 (1985).
[112] T. Blake, G. Lanfranchi, and D. M. Straub, Prog. Part. Nucl. Phys. **92**, 50 (2017).